Tracing provenance and sediment fluxes in the Irrawaddy River basin (Myanmar)

Eduardo Garzanti, Jiang-Gang Wang, Giovanni Vezzoli and Mara Limonta

Keywords:
Sand petrology
Heavy minerals
Bulk-sediment geochemistry Detrital zircon U-Pb geochronology Stream-profile analysis
Tectonic geomorphology

Abstract

This study illustrates the petrographic, heavy-mineral, geochemical and geochronological signatures of sand transported by various branches of the Irrawaddy (Ayeyarwadi) River, one of the first in the world for sediment flux. Intrasample and intersample compositional variability, weathering and hydraulic-sorting controls are also discussed. Feldspatho-quartzose sand in Irrawaddy headwaters is largely derived first-cycle from mid-crustal metamorphic and plutonic rocks of the Mogok Belt and Lohit complex, whereas feldspatho-litho-quartzose Chin- dwin sand is largely recycled from supracrustal, sedimentary and very low-grade metasedimentary units. Addi- tional mafic to ultramafic detritus is derived from ophiolites and blueschists exposed from the Indo-Burman Ranges to the Jade Mines and Myitkyina belts, linked northward to the Yarlung-Tsangpo suture of the Himalaya. Volcanic detritus derived from the Popa-Wuntho arc or recycled from forearc-basin strata also occurs. Decreasing concentration of most chemical elements along the Irrawaddy reflects progressive addition of detritus recycled from sedimentary rocks, most evident downstream of the Chindwin confluence. REE patterns with LREE enrich- ment and negative Eu anomaly reflect the occurrence of allanite, largely derived from granitoid rocks in the Mali catchment. Chemical indices indicate moderate weathering in the monsoon-dominated climate of Myanmar. Young U-Pb ages (15–170 Ma) represent 85% of detrital zircons in Irrawaddy headwater branches, reflecting long-lasting subduction-related magmatism along a ring of fire connecting with the southern and central Lhasa batholiths in Tibet and polyphase metamorphism in the Mogok belt. Chindwin sand contains larger amounts of finer-grained, recycled pre-Mesozoic zircons, also yielding early Mesoproterozoic to Archean ages. Such different petrographic, heavy-mineral, geochemical and geochronological fingerprints characterizing sand in different river branches allowed us to calculate bulk-sediment and zircon-provenance budgets that converge to indicate equivalent sand supply from the Nmai and Mali Rivers to the upper Irrawaddy, and from the Chindwin and upper Irrawaddy to the lower Irrawaddy. This implies that despite of higher erosion potential indicated by stream-profile analysis in high-relief Irrawaddy headwaters, sediment yields and erosion rates are

detectably higher in the Chindwin catchment, which is mainly ascribed to higher erodibility of widely exposed siliciclastic rocks. Quantifying sediment provenance and defining erosion patterns based on an integrated compositional da- tabase in a big-river system such as the mighty Irrawaddy allows us to expand our understanding of sediment- generation processes with the ultimate goal to increase our capacity to read into the stratigraphic record.

1.Introduction

Geological, geomorphological and sediment-generation processes in big-river catchments can be investigated by several different methods (e.g., Gaillardet et al., 1999; von Blanckenburg, 2005; Borges et al., 2008; Hinderer, 2012; Clift, 2015). The compositional and geochrono- logical signatures of detritus derived from an orogenic domain, which depend primarily on the lithology and time structure of source rocks and their evolution during progressive unroofing, provide an effective means to trace erosion processes in space and time (Garzanti, 2016). Any detrital component and any type of fingerprint (e.g., petrographic, mineralogical, geochemical, isotopic, geochronological) can be used as a provenance tracer to partition the sediment flux into its different sources (Padoan et al., 2011; von Eynatten and Dunkl, 2012), and hence to calculate average denudation rates in different parts of a river catchment once the total sediment load is known with reasonable accu- racy (Bouchez et al., 2011; Syvitski and Kettner, 2011). Quantitative geomorphological techniques, such as the analysis of stream profiles and their deviation from equilibrium, represent an excellent indepen- dent tool to constrain such estimates, allowing us to identify those areas where river tracts are in disequilibrium, and thus most likely to have undergone recent uplift and rapid exhumation (Castelltort et al., 2012; Kirby and Whipple, 2012; Willett et al., 2014; Vezzoli et al., 2014, 2016). The Irrawaddy (Ayeyarwadi) River, second in Indochina to the Me- kong but third in the world for sediment flux according to Robinson et al. (2007), drains most of northern and central Myanmar, a region segregated for long by a military dictatorship that only in recent years has tolerated democratic elections and gradual transition to more open so- ciety. Limited information has been consequently made available on this huge river system, including a few data on detrital mineralogy, geochemistry and geochronology (Bodet and Schärer, 2000; Garzanti et al., 2013a; Limonta et al., 2016). And yet knowing the composition and compositional variability of Irrawaddy sediments is crucial to solve provenance problems such as the origin of turbiditic clastic wedges exposed along the eastern side of the Himalayan collision zone (Allen et al., 2007) and the evolution of big-river systems in south-eastern Asia (Robinson et al., 2014; Licht et al., 2016). In this article we combine high-resolution petrographic, heavy-mineral, bulk-sediment geochemistry and U-Pb detrital-zircon geochronology analyses on modern sands collected in the entire Irrawaddy basin to assess the detrital fingerprints specific of principal tributaries and differ- ent trunk-river tracts (Fig. 1). Constrained further by the morphometric study of river profiles, this integrated database allows us to quantify sediment provenance and outline erosion patterns across the wide Irra-

waddy catchment.

2.The Irrawaddy River

2.1. Hydrology and sediment flux

The Irrawaddy (Mali-Nmai-Hka for Kachin natives) originates at 150 m a.s.l. in Kachin State from the confluence of the wilder Nmai Hka (“bad river”) and the quieter Mali Hka (“big river”) more navigable despite its lower discharge (Stamp, 1940). Both headwater branches are sourced from high mountain glaciers at ~28°N in northernmost Myan- mar, ~280 km SE of the eastern Himalaya syntaxis (Fig. 1A). The Irra- waddy (drainage basin ~430,000 km2) flows southward across Myanmar for ~ 2170 km and empties through a delta with nine arms into the Andaman Sea. Average and maximum water discharge are esti- mated to be 13,000 m3/s and 32,600 m3/s, and annual suspended load to be as high as 364 ± 60 ·106 tons (Robinson et al., 2007). An annual water discharge of 379 ± 47 km3 and a suspended-load flux of 325 ± 57·106 tons, with a significant decrease compared to the previous cen- tury, was calculated by Furuichi et al. (2009), based on data collected between 1969 and 1996 at Pyay well upstream of the delta. Its major Chindwin tributary (length ~ 1050 km, drainage basin ~ 115,000 km2) has an annual discharge of ~165 km3, reaching 300 km3 in severe flood years (Zin et al., 2009; Chapman et al., 2015). Most of the Irrawaddy basin is characterized by tropical monsoonal climate. Average temperatures in central Myanmar range between 25 °C and 30 °C during the wet season from May to October, when strong winds blow from the southwest bringing thunderstorms and heavy rain almost every day. They fall to 20–24 °C in the cold-dry season from November to February, and rise to 30–35 °C during the hot-dry season in March and April. Coastal regions may receive N 5 m of rain an- nually, decreasing to ~2.5 m in the delta (2.7 m at Yangon) and to 0.5– 1 m in the central plain (0.84 m at Mandalay). Annual precipitations in- crease up to ~ 4 m on the northern peaks, where climate is much cooler and snow falls in late autumn to early winter. The Irrawaddy upstream of the Chindwin confluence (named “upper Irrawaddy” throughout this article) is joined progressively by the Taping, Shweli and Myitnge left-bank tributaries and by the Mu right-bank tributary. The Chindwin River, also sourced in northern Myanmar, runs southward along the eastern edge of the Indo-Burman Ranges, receives its right-bank Myitha tributary (Myit is “river” in Bur- mese), and finally joins the Irrawaddy in the middle of the central Myanmar forearc basin. Only minor tributaries contribute to the lower Irrawaddy between the Chindwin confluence and the sea.

The Irrawaddy is still a natural system scarcely affected by human activities. Only the Ava bridge, built by the British in 1933 near Sagaing, existed on the river until 1998. In 2007, Myanmar's military dictatorship signed an agreement for the construction of seven hydroelectric dams in the Nmai and Mali Rivers, including the large Myitsone Dam at their confluence. Construction began in 2009 but was suspended in 2011 after the harsh

opposition of local communities and environmental organisations, concerned by the huge flooding area, relocation of ~15,000 people, earthquake hazards and ecological impact on biodi- verse ecosystems. Two major dams exist along the Shweli (Shweli-1, 2008) and Myitnge Rivers (Yeywa Dam, 2010), but none along the Chindwin River.

2.2. Geology of river catchments

The Nmai River drains the Mogok metamorphic belt, consisting of amphibolite-facies gneisses and schists with diopside-bearing marbles, migmatites and granitoid intrusions, passing south-eastwards to lower- grade garnet and chlorite schists, and finally to Neoproterozoic turbi- dites and Paleozoic sedimentary rocks of the Shan Plateau (Bertrand and Rangin, 2003). The tectonic evolution of the Mogok Belt is still unclear. The available radiometric ages indicate two metamorphic events at least, one before and one after the intrusion of Upper Jurassic/Lower Cretaceous granitoids (Barley et al., 2003; Mitchell et al., 2007, 2012). The Mali branch drains mainly into the quartz-diorites and associated intrusives of the Lohit Plutonic Complex (Gururajan and Choudhuri, 2003), representing the eastward continuation of the Gangdese batho- lith of south Tibet (Lin et al., 2013; Fig. 2).
The Taping and Shweli tributaries have their headwaters in the N/S- trending Gaoligong Belt, running adjacent to the Salween (Nujiang) river valley and welding the Tengchong and Baoshan Blocks (Zhao et al., 2016). Instead, the Myitnge River drains entirely within the northern Shan Plateau (Fig. 1B), south-east of the southward continuation of the Nujiang suture. The Shan Plateau exposes a thick stratigraphic succes- sion including Upper Cambrian siliciclastic and volcanic rocks, Ordovician to Devonian carbonates, black shales and quartzose sandstones, unconformably overlain by mid-Permian to mid-Triassic plateau lime- stones and followed in turn by Upper Triassic to Jurassic turbidites, limestones, shales and coal-bearing strata. Exposed along the N/S- trending Shan scarp to the west are locally metamorphosed Carboniferous-Lower Permian diamictites and folded Upper Jurassic to Lower Cre- taceous clastic rocks and limestones. The Mu River flows along the central Myanmar forearc basin and is sourced in the largely Upper Cre- taceous Wuntho Arc, correlative with the Lohit Plutonic Complex and the Gangdese batholith (Mitchell et al., 2012). The Chindwin River incises into the Cretaceous to Cenozoic forearc- basin fill of central Myanmar (Oo et al., 2015), but also drains basement gneisses and the Jade Mines Belt in headwater reaches (Shi et al., 2014) and receives much of its sediments from Paleogene remnant-ocean tur- bidites of the Indo-Burman Ranges before cutting across largely Plio-Pleistocene arc-related volcanic rocks near Monywa (Stephenson and Marshall, 1984). Its Myitha tributary drains entirely within the retro-side of the Indo-Burman Ranges, where Upper Triassic flysch and ophiolites are exposed between Paleogene deep-water turbidites in the west and the Kabaw Fault in the east. The latter may represent the southeastern prolongation of the Indus-Yarlung ophiolitic suture zone of the Himalaya (Fig. 2).

3.Sampling and analytical methods

In 2005 and 2013, 16 fine to medium sand samples were collected from active fluvial bars of the Irrawaddy River and its major tributaries in politically and logistically accessible areas from northern Myanmar headwaters to the mouth. Three silty levee sands (proxy for deep suspended load) and one mud sample (proxy for shallow suspended load) were also collected in the final tract.

3.1. Petrography and heavy minerals

A quartered fraction of each sand sample was impregnated with Araldite, cut into a standard thin section stained with alizarine red to distinguish dolomite and calcite, and analysed by counting 400 points under the microscope (Gazzi-Dickinson method; Ingersoll et al., 1984). Silty levee sands were wet sieved at 63 μm to eliminate the mud frac- tion. Sands were classified by their main components exceeding 10% QFL (Garzanti, 2016). Full quantitative information was collected on coarse-grained rock fragments, and their average metamorphic rank in each sample was expressed by Metamorphic Indices MI and MI*. MI varies from 0 (detritus shed by sedimentary and volcanic cover rocks) to 500 (detritus shed by high-grade basement rocks), whereas MI* considers only metamorphic rock fragments and thus varies from 100 (very- low-rank detritus shed by very low-grade metamorphic rocks) to 500 (Garzanti and Vezzoli, 2003). Very low- to low-rank metamorphic lithics, for which protolith can still be inferred, are subdivided into metasedimentary (Lms) and metavolcanic (Lmv) categories. Medium- rank to high-rank metamorphic lithics are subdivided into felsic (Lmf) and mafic (Lmb) categories. Median grain size was determined in thin section by ranking and visual comparison with sieved standards. Heavy-mineral analyses were mostly carried out on the 15–500 μm or >15 μm size fraction obtained by wet sieving. The 32–355 μm fraction was analysed on two bar sands; two silty levee sands were analysed in bulk. From a quartered aliquot of each sample, heavy minerals were separated by centrifuging in Na polytungstate (density ~2.90 g/cm3) and recovered by partial freezing with liquid nitrogen. Between 200 and 250 transparent heavy minerals were point-counted under the mi- croscope at suitable regular spacing to obtain real volume percentages (Galehouse, 1971). The HMC and tHMC (Heavy Mineral Concentration and transparent Heavy Mineral Concentration) indices were calculated as the volume percentage of total and transparent heavy minerals in the sediment. Heavy-mineral suites range from “very poor” (0.1 ≤ tHMC b 0.5) and “poor” (0.5 ≤ tHMC b 1) to “rich” (5 ≤ tHMC b 10), “very rich” (10 ≤ tHMC b 20) and “extremely rich” (20 ≤ tHMC b 50). The SRD (Source Rock Density) index, used as an es- timator of the average density of source rocks, is the weighted average density of terrigenous grains (Garzanti and Andò, 2007). Detrital components in each river tract are listed in order of abun- dance throughout the text. Key parameters are shown in Table 1; the complete petrographic and heavy-mineral datasets are provided in Tables A2 and A3.

3.2. Geochemistry

Chemical analyses were carried out at ACME Laboratories (Vancou- ver) on the 63–2000 μm fraction obtained by wet sieving for bar sands, on the bulk sample for silty levee sands, and on the b 32 μm frac- tion obtained by wet sieving for the mud sample. Major oxides and some minor elements were determined by ICP-ES and trace elements by ICP-MS, following a lithium metaborate/tetraborate fusion and nitric acid digestion. For further information on adopted procedures, geo- standards used and precision for various elements see http://acmelab. com (group 4A–4B and code LF200). To estimate weathering we used several chemical indices, including the Chemical Index of Alteration (CIA = 100 · A12O3 / (A12O3 + CaO + Na2O + K2O); Nesbitt and Young, 1982) and the Weathering Index (WIP = 100 · (CaO/0.7 + 2Na2O/0.35 + 2K2O/ 0.25 + MgO/0.9); Parker, 1970), calculated using molecular proportions of mobile alkali and alkaline earth metals corrected for Ca in apatite. No correction for Ca in carbonates was required because carbonate grains are virtually lacking in Irrawaddy sediments (Table A2). The ratio be- tween the CIA (a truer indicator of weathering) and the WIP (strongly influenced by quartz dilution) was used as an indicator of recycling (Garzanti et al., 2014). Weathering intensities were calculated for each single mobile element by comparing its concentration to that of nonmobile Al in our samples and in the Upper Continental Crust standard (UCC; Rudnick and Gao, 2003; Hu and Gao, 2008) (αAlE = (Al/E)sam- ple/(Al/E)UCC; Garzanti et al., 2013b, modified after α values of Gaillardet et al., 1999). Rare earth elements (REE) were normalized to CI carbonaceous chondrites (McDonough and Sun, 1995). Key parame- ters and weathering indices are shown in Table 2; the complete geochemical dataset is provided in Table A4.

3.3. Detrital zircon geochronology

From the dense fraction of nine samples obtained by elutriation, dense-liquid and magnetic-separation techniques, individual zircon grains were handpicked randomly, mounted in epoxy resin and then polished to produce a smooth, flat surface. Cathodoluminescence (CL) images were obtained to reveal internal structures and to select spots for U-Pb age analyses, conducted at the State Key Laboratory of Litho- sphere Evolution, Institute of Geology of Geophysics, Chinese Academy of Sciences. About 100 grains were analysed for each sample. U-Pb dat- ing was performed via LA–ICP–MS (instrumental conditions and data acquisition methods described in Xie et al., 2008). A spot diameter of 44 μm was used. The raw count rates for 204Pb, 206Pb, 207Pb, 208Pb, 232Th and 238U were collected for age determination. The 207Pb/206Pb and 206Pb/238U ratios were calculated using the GLITTER program (GEMOC, Macquarie University; Griffin et al., 2008). We used 206Pb/238U and 207Pb/206Pb ages for zircons younger and older than 1000 Ma, respectively, and did not consider in our provenance interpre- tation ages N500 Ma with >10% discordance nor ages b500 Ma with N30% discordance. The geochronological dataset is provided in Table A5.

3.4. Stream-profile analysis

The fluvial network was delineated in TecDEM (software shell im- plemented in MATLAB; Shahzad and Gloaguen, 2011) from a 30 m res- olution digital elevation model (DEM) provided by ASTER GDEM (http://www.gdem.aster.ersdac.or.jp). Concavity and steepness indices were calculated for 13 stream segments, including the main headwater branches and all major tributaries of the upper Irrawaddy and Chindwin Rivers. The Lohit River was also included for comparison.

4. Detrital fingerprints

In this section we shall illustrate first the petrographic, heavy-miner- al, geochemical and geochronological signatures of Irrawaddy sands, and discuss next the compositional modifications associated with physical (hydraulic sorting) and chemical (weathering) processes. Mechanical breakdown, demonstrated to be scarcely effective during fluvial transport (Russell, 1937; Garzanti et al., 2015a, 2015b), is not considered here.

4.1. The upper Irrawaddy

The Nmai and Mali Rivers carry litho-feldspatho-quartzose metamorphiclastic and feldspatho-quartzose plutoniclastic sands, re- spectively (Fig. 3A,B). Detrital modes and hornblende-epidote-garnet- clinopyroxene heavy-mineral assemblages are similar overall (Fig. 4), but only Nmai sand yields a few serpentinite grains, orthopyroxene and olivine, indicating minor contribution from ultramafic rocks. Metamorphic indices MI and MI*, measuring the average metamorphic rank of rock fragments, are higher in Mali sand, whereas heavy-mineral con-centration is much higher in Nmai sand (Table 1). Abundance of mafic minerals in Nmai sand is reflected by much higher Cr and Ni, and higher Fe, Mg, Ca, Sr, Sc, Ti, V, Mn and Co, whereas Mali sand shows higher K, Rb, Y, REE, Th, U, Nb, Ta and Sn (Fig. 5A). The marked LREE enrichment and strongly negative Eu anomaly in Mali sand is ascribed to the pres- ence of allanite, derived from granitoid source rocks (Fig. 6A). Upper Irrawaddy sand is feldspatho-quartzose (Fig. 3C). Plagioclase prevails slightly over K-feldspar. Rock fragments include granitoid, gneiss, micaschist, amphibolite, metasandstone, low-rank metabasite and a few siltstone/sandstone, shale/slate, phyllite, felsic volcanic and ultramafic grains. Micas are abundant, with dominant biotite. Rich, hornblende-dominated heavy-mineral assemblages include epidote and garnet, minor clinopyroxene, actinolite, titanite, and rare enstatite, olivine, hypersthene, Cr-spinel, apatite, sillimanite, staurolite, vesuvian- ite and allanite. Detrital modes change slightly from Myitkyina to Sagaing, where quartz and K-feldspar increase whereas metamorphic indices and heavy-mineral concentration progressively decrease (Table 1). This is reflected by a significant change in chemical composi- tion, with a decrease in all elements not hosted largely in quartz or K- feldspar; only Si increases, and to a lesser extent K and Ba (Fig. 5A). Detrital zircons are relatively coarse-grained in the upper Irrawaddy,

suggesting mainly plutonic sources. In Nmai, Mali and Irrawaddy sand downstream of the Nmai-Mali confluence half of zircon grains yielded U-Pb ages between 20 and 75 Ma, with peaks at 45–55 Ma and 59– 71 Ma (13% and 26% of total zircons, respectively). Another common cluster occurs between 128 and 151 Ma (11%). Nmai sand is character- ized by an additional cluster at 78–111 Ma (28% of zircons) and only 8 ages older than 151 Ma (1 at 405 Ma, 7 between 889 and 1144 Ma). Mali sand, instead, shows additional clusters at 15–20, 111–127 and 153–207 Ma (6%, 10% and 24%, respectively), with 8 ages scattered be- tween 314 and 1332 Ma (Fig. 7). Downstream changes are minor as far as Sagaing, where 7% of U-Pb zircon ages cluster at 21–36 Ma, 48% at 43–71 Ma, and 29% at 76– 211 Ma. Older ages cluster at 511–572 Ma (3%) and 987–1220 Ma (11%), with a single grain aged 3421 Ma. Data by Bodet and Schärer (2000) on only 37 grains from a sample collected at Mandalay showed clusters at 45–82 Ma (35%), 121–170 Ma (24%) and 1068–1099 Ma (12%), with a few grains at 3–23 Ma, 465–487 Ma and 1234–1397 Ma.

4.2. The Chindwin

The Chindwin River upstream of the Myitha confluence carries feldspatho-litho-quartzose sand (Fig. 3D). Plagioclase and K-feldspar are equally abundant. Rock fragments are mainly shale/slate, siltstone/sandstone, granitoid, gneiss and schist, with a few felsitic and microlitic volcanic, phyllite/schist and ultramafic grains (Fig. 4). Metamorphic in- dices are much lower than for upper Irrawaddy sands (Table 1). Micas were not observed. Heavy-mineral assemblages are moderately poor and dominated by amphiboles and epidote with subordinate garnet, minor rutile, staurolite, kyanite, Cr-spinel, and rare glaucophane, zircon, tourmaline, apatite and chloritoid. The Myitha tributary carries quartzo-lithic sand (Fig. 3E). Rock fragments are dominantly shale/slate and siltstone/sandstone/ metasandstone, with a few felsitic, microlitic and very-low-rank metavolcanic grains. Metamorphic indices are very low, half as those in Chindwin sand. The very poor heavy-mineral assemblage includes enstatite, clinopyroxene, epidote, amphibole, garnet, hypersthene, minor zircon, Cr-spinel, and rare apatite, andalusite and rutile. Abundant shale/slate rock fragments and occurrence of mafic minerals are reflected in relatively high concentration of Fe, Mg, Sc, Ti, V, Cr, Mn, Co, Ni and P. The composition of Chindwin sand changes little downstream of the Myitha confluence, but the MI* index decreases and the heavy mineral assemblage, still dominated by amphibole and epidote, becomes poorer and includes significant enstatite and clinopyroxene, somewhat more common garnet, and rare andalusite. More abundant quartz and poorer heavy-mineral assemblage than in upper Irrawaddy sand are reflected in much higher Si, whereas all other elements but Ni are less abundant (Fig. 5A). Many detrital zircons in Chindwin samples collected upstream and downstream of the Myitha confluence are very small and prob- ably recycled mainly from the Indo-Burman Ranges, but a few large grains probably eroded from the Wuntho batholith also occur. U-Pb ages cluster at 20–169 Ma (53%), 495–671 Ma (15%), 949–974 Ma (3%) and 1019–1191 Ma (10%). Other ages are scattered between 178 and 473 Ma (9%), between 693 and 895 (5%), and between 1213 and 3448 Ma (6%). One very young

age (1.0 ± 0.1 Ma) was also obtained, documenting provenance from Pleistocene volcanic products. Zircon grains in Myitha sand, mostly recycled from the Indo-Burman Ranges, cluster at 64–74 Ma (15%), 83–107 Ma (29%), 509–617 Ma (21%), 667–706 Ma (5%) and 1166–1209 (4%); the youngest 3% ranges between 44 and 57 Ma, and the oldest 10% is scattered between 1252 and 3338 Ma (Fig. 7).

4.3. The lower Irrawaddy

Irrawaddy sand downstream of the Chindwin confluence ranges from feldspatho-litho-quartzose to litho-feldspatho-quartzose (Fig. 3F). Plagioclase prevails slightly over K-feldspar, which includes perthitic and cross-hatched microcline. Rock fragments are mainly shale, siltstone/sandstone, slate, metasiltstone/metasandstone, phyllite, schist and paragneiss. Felsitic and subordinately microlitic volcanic, metavolcanic and metabasite (metarhyolite/metadacite, chloritoschist, epidosite, amphibolite), radiolarian chert and a few cellular serpentinite and serpentineschist grains also occur. Metamorphic indices are closer to those in Chindwin than in upper Irrawaddy sands, and decrease pro- gressively downstream. Micas are common, with dominant biotite. Moderately rich heavy-mineral assemblages include mainly amphiboles (including minor actinolite, rare oxy-hornblende and glaucophane) and epidote, with garnet, minor clinopyroxene, titanite, chloritoid, apatite, and rare enstatite, hypersthene, allanite, Cr-spinel, kyanite, staurolite, sillimanite, olivine, andalusite and monazite. Chemical composition is intermediate between that of Chindwin and upper Irrawaddy sands, but some elements (e.g., Cr and Ni) are no- tably enriched relative to both. Irrawaddy sand is markedly richer in Cr and Ni than the UCC standard and Ganga-Brahmaputra sand, and poorer in Ca and REE (Fig. 8). This reflects significantly greater contributions from mafic and ultramafic suture-zone and volcanic-arc rocks than for Himalayan-derived sediments, less metamorphic versus sedimentary detritus and hence less heavy minerals, and lack of carbonate grains. LREE-enrichment in lower Irrawaddy sands (Fig. 6) is chiefly ascribed to the presence of allanite, derived mainly from the Mali headwaters and an order of magnitude more common than monazite. Larger zircons from the Bagan sample and smaller zircons from the Nyaungdoun sample yielded main U-Pb age clusters at 18–76 Ma (36%), 84–128 Ma (26%), 138–154 Ma (4%), 510–574 Ma (7%), 638 Ma (2%) and 1019–1191 Ma (10%). Other ages are scattered be- tween 163 and 479 Ma (6%), between 710 and 994 Ma (5%) and be- tween 1180 and 1727 Ma (2%). The youngest and oldest ages resulted to be 0.5 Ma and 2609 Ma (Fig. 7). These data are comparable with those obtained from sample S3198 collected in a giant sandbar at Pyay and analysed by LA-ICP-MS at the London Geochronology Centre by Andrew Carter, where the main U-Pb clusters resulted to be 22–71 Ma (23%), 82–112 Ma (10%), 120–208 Ma (8%), 496–633 (15%) and 776– 1246 Ma (34%), with other ages scattered between 235 and 338 Ma (4%), and between 1476 and 2060 Ma (5%; Limonta et al., 2016).

4.4. Size-dependent intersample and intrasample compositional variability

To quantify differences in composition among samples, we collected very fine silty levee sands and fine to medium sand bars in three different localities along the lower Irrawaddy (B, C, E in Fig. 1A). Very fine levee sands have less quartz and K-feldspar and more mica, but intersample mineralogical variability is not prominent, as shown in Table 1. Heavy- mineral concentration is similar, but the epidote/amphibole ratio is higher in levee sands, and garnet less (Fig. 4). Greater abundance of quartz and K-feldspar is reflected by slightly higher concentrations in Si, K and Ba in coarser sand bars, whereas all other elements but Rb, Cr and W are more abundant in silty levees (Fig. 5B). In both levee and bar sands chon- drite-normalized REE patterns display the classical enrichment in light rare earth elements (LREE), negative Eu anomaly, and flat distribution of heavy rare earth elements (HREE; Fig. 6B).
Our mineralogical and geochemical datasets do not show evidence of strong selective-entrainment effects. The SRD index (i.e., estimated grain density) is high only in the heavy-mineral enriched Nmai sand, where Th and Cr are higher by factors of 3–5 relative to the UCC stan- dard, and Fe, Ti, LREE, U, Zr, Hf higher by factors of 1.5–2. This is partly a provenance effect, because SRD indices of 2.76–2.78 characterize both uppermost Irrawaddy samples collected just downstream of the Nmai-Mali confluence, where most element concentrations are close to the average of Nmai and Mali sands, only Fe, LREE, Th, U, Ti, V, Mn and Cr being 20–40% lower (Table 2). SRD indices decrease progressively downstream with decreasing heavy-mineral concentra- tion as far as the mouth (Table 1). To quantify intrasample compositional variability (i.e., differences among different size classes of the same sample), one well-sorted lower-fine bar sand (sample 3200FS) was sieve-split into three 0.5 ϕ classes, representing 97.4 wt% of the bulk sample; each class was analysed separately for petrography, heavy-minerals and geochemistry. As predicted by the settling-equivalence principle (Rubey, 1933; Garzanti et al., 2008), the 80–125 μm class (17.9 wt%) is heavy-mineral rich, whereas the 125–180 μm class (67.8 wt%) and the 180–250 μm class (11.7 wt%) contain moderately poor and very poor heavy-mineral assemblages, respectively. The 180–250 μm class is markedly enriched in altered biotite and muscovite. Geochemically, such variability is reflected by concentration of elements chiefly hosted in dense minerals in the fine tail of the size distribution (Ca, Sc, Y, REE, Th, U, Zr, Hf, V, Ti, Nb, Ta, Cr, Mn, Sn and P), and of elements associated with micas in the coarse tail (K, Rb, Ba, Co and Ni; Fig. 5B). The densest minerals (i.e., zir- con, rutile, Cr-spinel, kyanite and chloritoid) were observed only in the 80–125 μm class, where ultradense magnetite and ilmenite are concen- trated markedly (Fig. 9). Conversely, less dense amphiboles are relative- ly enriched in the 180–250 μm class, where ultradense garnet becomes rare and slow-settling micas most abundant. As a typical settling-equivalence effect (Garzanti et al., 2010), the Eu anomaly is strongly negative in the 80–125 μm class and only slightly negative in the 125– 180 μm and 180–250 μm classes (Fig. 6B).

4.5. Chemical weathering

Chemical parameters such as the CIA or αAl values are widely used to infer weathering conditions in source areas, although they are con- trolled markedly by the mineralogy of

source rocks and inheritance from previous sedimentary cycles (Borges et al., 2008; Garzanti and Resentini, 2016). Moreover, bedload sand is far less sensitive to weathering than mud carried in suspension, for which more extensive information is available (Li and Yang, 2010; Shao et al., 2012). Singling out the weathering signal from provenance, recycling and grain-size noises is thus far from straightforward. For instance, αAlMg, αAlCa and αAlSr are b1 and αAlK, αAlRb and αAlBa N 1 in Nmai sand, where mafic/ultramafic detritus is significant and heavy minerals very abun- dant. Precisely the opposite occurs in Mali sand, indicating different par- ent lithologies (i.e., mainly metamorphic Mogok Belt for the former, mainly Lohit Plutonic Complex for the latter), rather than different cli- matic conditions in these two adjacent catchments. All chemical indices but αAlMg are highest in Myitha sand, and particularly αAlCa (4.1) and αAlSr (3.5), pointing to provenance from mudrocks originally depleted in Ca and Sr. The CIA/WIP ratio for Chindwin sands (2.3 ± 0.1) is double than for upper Irrawaddy sands (1.0 ± 0.1), reflecting much more ex- tensive recycling of siliciclastic units in the catchment of the former (Table 2). Irrawaddy sands in the headwaters have αAlNa 1.4–1.5 and αAl indi- ces ≤ 1.2 for other mobile elements, testifying to mainly physical erosion with moderate weathering effects. Stronger weathering is indicated for northwestern Myanmar and the Indo-Burman Ranges, where αAlK, αAlRb and αAlBa range between 1.4 and 3.2, and αAlNa is 1.8 in Chin- dwin sand and 2.1 in Myitha sand. Further indication of significant weathering is the lack of soluble carbonate grains in Irrawaddy sands, absent also in Brahmaputra sediments but common in Ganga sands and abundant in Indus sands (Fig. 4 in Garzanti et al., 2005; Table 3). Scarcely exposed in the rest of the Irrawaddy catchment, carbonate rocks do occur in the Paleozoic-Mesozoic succession of the Shan Plateau, which however does not appear to supply much sediment also because of extensive karst (Dreybrodt et al., 2013). CIA values are 52.6 ± 0.2 for upper Irrawaddy sand, 57.0 ± 0.3 for Chindwin sand, 56.9 ± 0.9 for lower Irrawaddy sand (αAlNa 1.6 ± 0.2), 63.6 ± 2.1 for lower Irrawaddy silty levees (αAlNa 1.8 ± 0.2), and 72 for lower Irrawaddy mud (αAlNa 3.4). Similar values are record- ed in the Ganga-Brahmaputra river system for sand bedload (CIA corrected for CaO in carbonates 55 ± 4; αAlNa 1.5 ± 0.2) and silty sand carried in suspension close to the bed (CIA 61 ± 3, increasing to 69 ± 5 for silty mud entrained close to the surface; Garzanti et al., 2011; Lupker et al., 2011). Higher values are reported for bedload sands of all other major rivers in Indochina (CIA 63 ± 3 and αAlNa 1.7 ± 0.5 for the Salween, CIA 71 ± 2 and αAlNa 3.7 ± 2.0 for the Me- kong, CIA 67 ± 3 and αAlNa 3.5 ± 2.2 for the Red River; Borges et al., 2008) and characterize smaller rivers in SE China (CIA 60 ± 2 and αAlNa 2.7 ± 0.8; Fig. 8). Northward decreasing weathering intensity is reflected by lower indices for Yangtze and Yellow River sands (CIA 59 ± 3 and αAlNa 1.7 ± 0.7, CIA 54 ± 3 and αAlNa 1.2 ± 0.1, respectively; Borges et al., 2008), both containing a significant amount of carbon- ate grains (Table 3). Despite the variety of problems involved in the use of chemical indi- ces of sediments to infer weathering conditions in a drainage basin, pet- rographic and chemical signatures of river sands concur to indicate that weathering effects, significant but not strong enough to affect sand composition severely in Myanmar, become progressively stronger

across southern Asia from dry Pakistan in the west to humid Indochina in the east, to decrease again with increasing latitude in eastern Asia (Yang et al., 2004; Shao et al., 2012).

5. Stream-profile analysis

Fluvial profiles are described by a power-law relationship between the local channel slope S and the contributing drainage area A used as a proxy for discharge, in the form S = ksA–θ (Flint, 1974). The chan- nel-steepness index ks is a measure of bedrock-channel response to dif- ferential rock uplift if other controls such as rock type, climate, flood hydrology or sediment flux are negligible or sufficiently constrained (Whipple and Tucker, 1999; Kirby et al., 2003). Steepness indices essen- tially integrate seismic activity and rock deformation over geological timescales, and higher values have been related to higher erosion and/ or exhumation rates (Ouimet et al., 2009). To facilitate comparison of gradients in channels with widely varying drainage areas, we used here the steepness index ksn normalized by a fixed reference concavity of 0.45 for all river segments (Korup and Schlunegger, 2009). The concavity index θ describes the rate of change of channel gradi- ent with drainage area. According to Whipple (2004), low concavities (θ b 0.4) are associated either with short steep drainage influenced by debris flows or with downstream increase in incision rate or rock strength, commonly related to knickpoints. Moderate concavities (θ 0.4–0.7) are associated with actively uplifting bedrock channels in homogeneous substrates experiencing uniform rock uplift. High con- cavities (θ 0.7–1.0) are associated with the downstream decrease in rock-uplift rate or rock strength. Extreme concavities (θ b 0 or N 1) are associated with abrupt knickpoints, related to either pronounced along-stream changes in substrate properties or spatial or temporal differences in rock-uplift rate, including transitions from incisional to depositional conditions.

5.1. Results

The Nmai River displays very low concavity and very high steepness, comparable only to that of the Lohit River and significantly higher than the Mali River (Fig. 10), thus indicating the highest erosion potential among all studied stream segments. Left tributaries of the upper Irra- waddy also display low concavities. Concavities close to 0 characterize the Shweli River, showing a major knickpoint where the lower course exits the Mogok Belt, and the Myitnge River, showing several knickpoints corresponding to faults or lithological boundaries between substrates with different erodibility in the stratigraphy of the Shan Plateau. Channel steepness is high for the Taping and Shweli Rivers draining the Gaoligong and Mogok Belts, and only moderate for the Myitnge River draining the Shan Plateau, where erosion potential is lower. Moderately low ksn and θ indices characterize headwater branches of the Chindwin River and its major tributaries draining the Indo-Burman Ranges. Slightly negative θ value for the Phek River reflects the presence of knickpoints where the lower course crosses the Kabaw Fault. The lowest ksn value is displayed by the Mu River flowing along the central Myanmar forearc

basin (Fig. 10).

6. Provenance and sediment budgets

6.1. Sources of sand

Metamorphiclastic and plutoniclastic sands supplied by the Nmai and Mali Rivers to the upper Irrawaddy reflects provenance from gran- itoids and amphibolite-facies metasedimentary and metaigneous rocks of the mid-crustal tectono-stratigraphic level exposed in the Mogok Belt and Lohit Plutonic Complex (Fig. 11). Additional metavolcanic to metabasite and ultramafic grains in Nmai sand are derived from greenschist-facies and subgreenschist-facies rocks and serpentinites ex- posed in the Myitkyina Belt (Mitchell et al., 2007), which connects along strike with the Tidding suture and finally with the Yarlung-Tsangpo su- ture zone west of the eastern Himalayan syntaxis (Fig. 2; Searle et al., 2007). Chindwin sand, characterized by much higher quartz/feldspar ratio and much lower metamorphic indices and heavy-mineral concentra- tion, is chiefly derived instead from supracrustal, sedimentary and very low-grade metasedimentary units. Occurrence of minor Cr-spinel and ultramafic rock fragments indicate additional supply from ophiolitic mantle rocks. Glaucophane grains point to provenance from blueschists of the Jade Mines Belt (Shi et al., 2014). Minor volcanic rock fragments are both recycled from central Myanmar forearc-basin strata and de- rived first-cycle from the Popa-Wuntho arc. Sedimentaclastic sand of the Myitha tributary reflects provenance mostly from unmetamorphosed to anchimetamorphic turbidites of the Indo-Burman Ranges (Garzanti et al., 2013a). The poor heavy-mineral assemblage includes pyroxenes and Cr-spinel derived ultimately from associated ophiolites and volcaniclastic rocks. Lower Irrawaddy sand shows intermediate composition between Chindwin and upper Irrawaddy sands. The slight progressive down- stream increase in volcanic rock fragments and chert, and the slight de- crease in metamorphic indices points to additional local supply from sedimentary and volcaniclastic cover rocks. Enrichment in elements such as Cr and Ni relative to upstream branches confirms addition of some recycled or even first-cycle volcanic detritus along the lower course. Dominantly young U-Pb zircon ages between 40 and 170 Ma from Irrawaddy headwaters to the mouth reflect long-lasting subduction-re- lated magmatic activity documented along two parallel belts, the southwestern one including the Wuntho Arc and the Lohit Plutonic Complex connecting with the Gangdese batholith in the southern Lhasa Block, and the northeastern one including the Dianxi and Bomi- Chayu batholiths connecting with the central Lhasa plutonic belt (Liang et al., 2013; Lin et al., 2013; Wang et al., 2014). Young U-Pb ages in a similar time window and ranging from as young as 17– 21 Ma to as old as 170 Ma also characterize intrusive and metamorphic rocks of the Mogok Belt (Barley et al., 2003; Searle et al., 2007; Mitchell et al., 2012). These are by far the main sources of zircon grains for upper Irrawaddy sand, zircon contributions from the Shan Plateau being bare- ly detected. The distinct very young 15–20 Ma and relatively old 153– 207 Ma peaks documented in Mali sand

may have a different prove- nance, possibly from the Katha-Gangaw Range and/or the Myitkyina belt. The one grain dated at 0.5 Ma in lower Irrawaddy sand at Bagan may have been derived from the Popa Volcano nearby. U-Pb zircon ages in Myitha sand match broadly the distributions re- ported in the available studies of the Indo-Burman Ranges. The usual dominant 42–150 Ma cluster with subordinate Cambro-Ordovician and Precambrian ages characterize Paleogene turbidites (Allen et al., 2008). Instead, zircon ages in Triassic turbidites are mostly between 480 and 1400 Ma, but several range between 200 and 300 Ma, a few fall in the 320–410 Ma and 1400–2100 Ma intervals, and some are >2500 Ma and as old as 3445 Ma (Sevastjanova et al., 2016). Chindwin zircons with ages between 23 and 36 Ma, between 125 and 170 Ma, and between 1000 and 1100 Ma have no equivalent in Myitha sand, and may be derived from headwater sources including gneisses of the Katha-Gangaw Range and high-pressure rocks of the Jade Mines Belt (Shi et al., 2014).

6.2. Bulk-sand provenance budget

The relative amount of bedload sand contributed by different tribu- taries to the Irrawaddy River can be assessed by forward mixing models based on either integrated bulk-petrography and heavy-mineral data or on geochemical data (Garzanti et al., 2012). The followed mathematical approach is illustrated in detail in Appendix A. The comparison of prov- enance budgets based on different datasets is indispensable to reduce the uncertainties of each, which are typically large wherever the com- positional signatures of the end members are not sharply distinct and/or replicate samples are not available. In order to verify outcome sensi- tivity, several sets of independent trials were carried out according to a range of different assumptions, and the mean and the standard deviation of the results obtained were calculated. Our calculations based on the petrographic, heavy-mineral, and integrated petrographic-heavy mineral datasets suggest that upper Irrawaddy sands are derived in subequal amounts from the Nmai (56 ± 13%) and Mali Rivers (44 ± 13%). Calculations based on geochemical data confirm comparable con- tribution from the Nmai (42 ± 21%) and Mali Rivers (58 ± 21%), with large uncertainties associated with different adopted criteria and selected chemical elements. Detrital modes change little along the upper Irrawaddy. Sand supply from tributaries downstream of the Nmai-Mali confluence is therefore subordinate, although it explains the slight increase in quartz and regu- lar progressive decrease in metamorphic indices and heavy-mineral concentration observed from Myitkyina to Sagaing. Geochemical trends clearly outline a depletion in most elements along this river tract (Fig.5A), ascribed to the additional detritus derived from sedimentary and metasedimentary rocks of the Shan Plateau. The Myitha River does not contribute much sand (≤ 10%) to the Chin- dwin River. The Chindwin resulted to supply the majority of bedload sand (62 ± 11%) to the lower Irrawaddy, and is thus inferred to repre- sent the major sediment-conveyor branch in the system. Although affected by even larger uncertainties, calculations based on geochemical data confirm conclusively that sand contribution of the Myitha tributary to the Chindwin is minor, and suggest comparable contributions from the Chindwin (46 ± 13) and upper

Irrawaddy (54 ± 13) to the lower Irrawaddy.

6.3. Zircon provenance budget

Detrital-geochronology offers an alternative way to evaluate the rel- ative sediment contribution from different fluvial branches, although sediment budgets based on single-mineral data suffer from major uncertainties and are thus intrinsically unrobust. Zircon provenance budgets need to be corrected by the zircon fertility of source rocks in each catchment (Malusà et al., 2015), which generally can be inferred only under the frail assumption that zircon concentration in the sedi- ment sample reflects faithfully zircon fertility in the source (i.e., that hydraulic sorting and other effects are negligible; Garzanti et al., 2009). Moreover, zircon concentration is very hard to assess precisely by opti- cal heavy-mineral analysis, because: a) the bulk sediment or at least a suitably large size class should be investigated to avoid cutting off the fine tail of the size distribution enriched in ultradense zircon because of settling-equivalence effects; b) point-counting should be used to ob- tain correct volume percentages; c) the concentration of total heavy minerals in the sample should be accurately measured; d) zircon should be a transparent heavy mineral sufficiently common in the sample that its relative concentration could be assessed precisely without counting an unreasonably large number of grains. Zircon concentration is more easily recalculated from geochemical data, under the assumption that zircon contains on average 465,000 ppm Zr and typically contributes between 60% and 80% of total Zr to fluvial sand (Garzanti et al., 2010). Detrital zircons in Nmai and Mali sands display U-Pb age spectra suf- ficiently distinct to evaluate their relative zircon contribution to the upper Irrawaddy. Calculations performed using different age classes and following different criteria suggest that zircons are derived in subequal amounts from the Nmai (47 ± 7%) and Mali Rivers (53 ± 7%). This zircon provenance budget could not be translated reliably into a bedload budget. Zircon grains are too few in both Nmai and Mali sands to calculate absolute zircon concentrations from heavy-min- eral data. The latter could be recalculated from geochemical data, but higher Zr is partly caused by hydrodynamic concentration of ultradense grains in the Nmai sample, as indicated by its very high SRD index (Table 1). Hydraulic sorting also explains the irregular fluctuations of Zr content in the two upper Irrawaddy samples collected south of the Nmai-Mali confluence (Table 2). Age spectra do not change significantly downstream the upper Irra- waddy, where no new age peak appears as far as Sagaing, apart from a single grain of Archean age. The potential contribution from tributaries draining the Shan Plateau thus remains beyond detection. Calculations performed for the lower Irrawaddy suggest that zircons are derived in similar amounts from the Chindwin (45 ± 22%) and upper Irrawaddy (55 ± 22%). Heavy-mineral and geochemical data consistently suggest higher zircon concentrations for upper Irrawaddy sand (0.02–0.03%) than for Chindwin sand (0.008–0.01%). Such corrections would imply a larger sand flux for the Chindwin (66 ± 18%) than for the upper Irra- waddy (34 ± 18%).

6.4. From provenance budgets to erosion rates

Despite the notable uncertainties associated with each, provenance budgets based on integrated petrographic and heavy-mineral data, on geochemical data, and on geochronological data provide consistent in- dications on relative sediment fluxes. All estimates converge to indicate equivalent sediment supply from the Nmai and Mali Rivers to the upper Irrawaddy (48 ± 14 vs. 52 ± 14, respectively) and from the Chindwin and upper Irrawaddy to the lower Irrawaddy (55 ± 17 vs. 45 ± 17, respectively). If our calculations are correct, then the total load carried annually on average by the Irrawaddy River to the sea, amounting to between 350 and 400 · 106 tons (including between 325 ± 57 and 364 ± 60 · 106 suspended load according to Furuichi et al., 2009 and Robinson et al., 2007, and between 30 and 40 · 106 bedload assumed to be ~10% of suspended load; Hay, 1998 p.297), can be roughly reapportioned as fol- lows: ~ 200 · 106 tons from the Chindwin; 60–70 · 106 tons each from the Nmai and the Mali, ~10 · 106 tons from the Taping, ~30 · 106 from the Shweli and ~5 · 106 from the Myitnge. The corresponding average sed- iment yields and erosion rates would be ~ 1300 tons/km2 · a and ~0.5 mm/a for the equally large Nmai and Mali catchments (thus much lower than in the adjacent Lohit catchment; Garzanti et al., 2004), and ~ 1700 tons/km2 · a and ~ 0.7 mm/a for the Chindwin catch- ment. Sediment yields and erosion rates would be ~ 1000 tons/km2 · a and 0.3–0.4 mm/a for both the upper Irrawaddy and the entire Irrawad- dy basin. This is consistent with cosmogenic 10Be measurements on quartz carried out on sample S3200FS by Hanna Haedke and Hella Wittman (GFZ Potsdam), pointing to catchment-wide erosion rates of 0.27 ± 0.03 mm/a averaging over millennial time scales. These estimates are based on the assumption that the provenance budget determined for bedload sand can be applied to suspended load equally, which is never fulfilled exactly. In river systems draining conti- nental flood basalts, including the Nile and right-bank tributaries of the Ganga (Garçon and Chauvel, 2014; Garzanti et al., 2015a), volcaniclastic sediments are notably finer-grained and transported preferentially in suspension, whereas detritus from basement rocks and cover strata is concentrated in bedload. On the one hand, volcanic sources are minor and size-dependent intersample mineralogical variability is not promi- nent in the Irrawaddy catchment (see Subsection 4.4), which indicates that the assumption may be acceptably fulfilled. On the other hand, we noticed that zircon grains tend to be notably smaller in the Chindwin branch than in the upper Irrawaddy. Because the ratio between the mud and sand generation potentials is expected to be significantly greater for turbidites exposed in the Indo-Burman Ranges than for tougher and coarser-grained gneisses and granitoids exposed in the Irrawaddy head- waters, Chindwin contribution is possibly under- represented in bedload. If this were true, then the sediment yields and erosion rates given above would be over-estimated for the upper Irrawaddy and under-estimated for the Chindwin. Lower average erosion rates in the Nmai and Mali catchments than in the Chindwin catchment are apparently at odds with the much lower steepness index of the latter. Because precipitations are comparable, the higher sediment yield in the Chin- dwin basin than in upper Irrawaddy headwaters despite a lower relief is mainly ascribed to the higher erodibility of

terrigenous rocks widely exposed in the Indo-Burman Ranges and in the rest of the Chindwin basin, which are unable to sustain rugged topography (Korup and Schlunegger, 2009). Some information on sediment supply and erosion rates in central and eastern Myanmar can be deduced from the compositional change observed along the upper Irrawaddy, coupled with channel-morphom- etry data on its main tributaries. The slight downstream increase in quartz and steady progressive decrease in metamorphic indices and heavy-mineral concentration indicates a significant, although subordi- nate contribution from sedimentary rocks. Information from sediment composition and stream-profile analysis converges to suggest for the Taping and Shweli catchments average sediment yields and erosion rates (1000–1500 tons/km2 · a and ~ 0.5 mm/a) similar to the Nmai and Mali catchments draining similar lithologies. Lower erosion rates are predicted for the Myitnge catchment (~ 200 tons/km2 · a and ~0.1 mm/a), also considering the widespread limestone exposures in the Shan Plateau (Fig. 1 in Dreybrodt et al., 2013). Lowest erosion rates are suggested for the central Myanmar forearc basin drained by the Mu River.

7. Summary and conclusion

In this article we have combined petrographic, heavy-mineral, geo- chemical and geochronological analyses of modern sands to trace sedi- ment provenance in the entire Irrawaddy (Ayeyarwadi) basin. Constrained independently by the morphometric study of river profiles, these integrated datasets allowed us to evaluate sediment-generation processes and explore erosion patterns across northern and central Myanmar. The Irrawaddy, still a natural system scarcely affected by human activities, ranks among the first in the world for its sediment load. Feldspatho-quartzose sand in the headwaters is chiefly derived from mid-crustal metamorphic and plutonic rocks of the Mogok Belt and Lohit Plutonic Complex exposed in the Nmai and Mali catchments southeast of the eastern Himalayan syntaxis. REE patterns with LREE en- richment and negative Eu anomaly reflect the occurrence of allanite, largely derived from granitoid rocks in the Mali catchment. Contribution from sedimentary rocks of the Shan Plateau and ophiolitic mélanges is subordinate. Feldspatho-litho-quartzose sand in the Chindwin River is derived instead principally from sedimentary to very low-grade metasedimentary supracrustal units of the Indo-Burman Ranges and central Myanmar forearc basin. Contributions from arc rocks of the Popa-Wuntho arc and blueschist to eclogite-facies ophiolites of the Jades Mine Belt are minor, but glaucophane is traced to as far as the Ir- rawaddy mouth in the Andaman Sea. Feldspatho-litho-quartzose to litho-feldspatho-quartzose sand in the lower Irrawaddy is calculated to be supplied a little more from the Chindwin tributary than from the upper Irrawaddy. The slight progressive downstream increase in volca- nic rock fragments and chert, and decrease in metamorphic indices, point to additional local recycling of sedimentary and volcaniclastic rocks in the lower reaches. Geochemical and petrographic signatures of river sands concur to indicate that weathering effects are significant but not strong enough to affect sand composition severely in mon-

soon-dominated Myanmar. U-Pb age spectra of detrital zircons are char- acterized by a major cluster at 30–150 Ma, corresponding to the long- lasting magmatic activity of the Western Myanmar Arc, with other clus- ters at 500–600 Ma and 800–1200 Ma, and a few ages between 1.5 and 2.0 Ga. Compositional differences between very fine-grained silty levee sands and fine to medium-grained fluvial bar sands are limited, with >90% intrasample variability explained by settling-equivalence effects. The detailed characterization of detrital fingerprints in various branches of modern big-river systems is essential to understand sediment-generation processes and to develop new concepts that may sharpen our capacity to interpret the vast amount of geological information stored in fossil clastic systems.

Acknowledgments
We are deeply grateful to the Editor Jerôme Gaillardet and two reviewers for their very useful comments and constructive criticism. Yani Najman travelled the lower Irrawaddy with EG in 2005. Andrew Carter, Christian France-Lanord, Hanna Haedke, Hella Wittman and Shouye Yang kindly provided geochronological and geochemical data. Work financially supported by the Strategic Priority Research Program (B) of the Chinese Academy of Sciences (XDB03010100).

References

- Andò, S., Morton, A., Garzanti, E., 2014. Metamorphic grade of source rocks revealed by chemical fingerprints of detrital amphibole and garnet. In: Scott, R., Smyth, H, Morton, A, Richardson, N (Eds.), Sediment provenance studies in hydrocarbon exploration and production. Geol. Soc. Lond. Spec. Publ. 386, pp. 351–371.
- Allen, R., Carter, A., Najman, Y., Bandopadhyay, P.C., Chapman, H.J., Bickle, M.J., Garzanti, E., Vezzoli, G., Andò, S., Foster, G.L., Gerring, C., 2007. New constraints on the sedimentation and uplift history of the Andaman–Nicobar accretionary prism, South Andaman Island. In: Draut, A., Clift, P.D., Scholl, D.W. (Eds.), Formation and Applications of the Sedimentary Record in Arc Collision Zones. Geological Society of America, Special Paper Vol. 436, pp. 223–255.
- Allen, R., Najman, Y., Carter, A., Barfod, D., Bickle, M.J., Chapman, H.J., Garzanti, E., Vezzoli, G., Andò, S., Parrish, R.R., 2008. Provenance of the Tertiary sedimentary rocks of the Indo-Burman ranges, Burma (Myanmar): Burman arc or Himalayan-derived? J. Geol. Soc. Lond. 165, 1045–1057.
- Barley, M.E., Pickard, A.L., Zaw, K., Rak, P., Doyle, M.G., 2003. Jurassic to Miocene magmatism and metamorphism in the Mogok metamorphic belt and the India–Eur- asia collision in Myanmar. Tectonics 22, 1019. http://dx.doi.org/10.1029/ 2002TC001398.
- Bertrand, G., Rangin, C., 2003. Tectonics of the western margin of the Shan plateau (cen- tral Myanmar): implication for the India–Indochina oblique convergence since the Oligocene. J. Asian Earth Sci. 21, 1139–1157.

- Bodet, F., Schärer, U., 2000. Evolution of the SE-Asian continent from U-Pb and Hf isotopes in single grains of zircon and baddeleyite from large rivers. Geochim. Cosmochim. Acta 64, 2067–2091.
- Borges, J.B., Huh, Y., Moon, S., Noh, H., 2008. Provenance and weathering control on river bed sediments of the eastern Tibetan plateau and the Russian Far East. Chem. Geol. 254, 52–72.
- Bouchez, J., Lupker, M., Gaillardet, J., France-Lanord, C., Maurice, L., 2011. How important is it to integrate riverine suspended sediment chemical composition with depth? Clues from Amazon River depth-profiles. Geochim. Cosmochim. Acta 75, 6955–6970.
- Castelltort, S., Goren, L., Willett, S.D., Champagnac, J.D., Herman, F., Braun, J., 2012. River drainage patterns in the New Zealand Alps primarily controlled by plate tectonic strain. Nat. Geosci. 5, 744–748.
- Chapman, H., Bickle, M., Thaw, S.H., Thiam, H.N., 2015. Chemical fluxes from time series sampling of the Irrawaddy and Salween rivers, Myanmar. Chem. Geol. 401, 15–27.
- Clift, P.D., 2015. Assessing effective provenance methods for fluvial sediment in the South China Sea. Geol. Soc. Lond. Spec. Publ. 429. http://dx.doi.org/10.1144/SP429.3.
- Clift, P.D., Giosan, L., Carter, A., Garzanti, E., Galy, V., Tabrez, A.R., Pringle, M., Campbell, I.H., France-Lanord, C., Blusztajn, J., Allen, C., Alizai, A., Lückge, A., Danish, M., Rabbani, M.M., 2010. Monsoon control over erosion patterns in the western Himalaya: possi- ble feed-back into the tectonic evolution. Geol. Soc. Lond. Spec. Publ. 342, 185–218.
- Dreybrodt, J., Furlong, I., Loveridge, F., Talling, P., 2013. Speleological expeditions to the Shan plateau in Myanmar. Proceedings of the 16th International Congress of Speleol- ogy, Brno, Czech Republic. Vol. 2, pp. 62–67.
- Flint, J.J., 1974. Stream gradient as a function of order, magnitude, and discharge. Water Resour. Res. 10, 969–973.
- Furuichi, T., Win, Z., Wasson, R.J., 2009. Discharge and suspended sediment transport in the Ayeyarwady River, Myanmar: centennial and decadal changes. Hydrol. Process. 23, 1631–1641.
- Gabriel, K.R., 1971. The biplot graphic display of matrices with application to principal component analysis. Biometrika 58, 453–467.
- Gaillardet, J., Dupré, B., Allègre, C.J., 1999. Geochemistry of large river suspended sedi- ments: silicate weathering or recycling tracer? Geochim. Cosmochim. Acta 63, 4037–4051.
- Galehouse, J.S., 1971. Point counting. In: Carver, R.E. (Ed.), Procedures in Sedimentary Petrology. Wiley, New York, pp. 385–407.
- Galy, V., France-Lanord, C., Beyssac, O., Faure, P., Kudrass, H., Palhol, F., 2007. Efficient organic carbon burial in the Bengal fan sustained by the Himalayan erosional system.

Nature 450, 407–410.

- Garçon, M., Chauvel, C., 2014. Where is basalt in river sediments, and why does it matter? Earth Planet. Sci. Lett. 407, 61–69.
- Garzanti, E., 2016. From static to dynamic provenance analysis — sedimentary petrology upgraded. Sediment. Geol. 336, 3–13.
- Garzanti, E., Andó, S., 2007. Heavy-mineral concentration in modern sands: implications for provenance interpretation. In: Mange, M.A., Wright, D.T. (Eds.), Heavy Minerals in UseDevelopments in Sedimentology Series Vol. 58. Elsevier, Amsterdam, pp. 517–545.
- Garzanti, E., Resentini, A., 2016. Provenance control on chemical indices of weathering (Taiwan river sands). Sediment. Geol. 336, 81–95.
- Garzanti, E., Vezzoli, G., 2003. A classification of metamorphic grains in sands based on their composition and grade. J. Sediment. Res. 73, 830–837.
- Garzanti, E., Vezzoli, G., Andó, S., France-Lanord, C., Singh, S.K., Foster, G., 2004. Sediment composition and focused erosion in collision orogens: the Brahmaputra case. Earth Planet. Sci. Lett. 220, 157–174.
- Garzanti, E., Vezzoli, G., Andò, S., Paparella, P., Clift, P.D., 2005. Petrology of Indus river sands: a key to interpret erosion history of the western Himalayan syntaxis. Earth Planet. Sci. Lett. 229, 287–302.
- Garzanti, E., Andó, S., Vezzoli, G., 2008. Settling-equivalence of detrital minerals and grain size dependence of sediment composition. Earth Planet. Sci. Lett. 273, 138–151.
- Garzanti, E., Andó, S., Vezzoli, G., 2009. Grain-size dependence of sediment composition and environmental bias in provenance studies. Earth Planet. Sci. Lett. 277, 422–432.
- Garzanti, E., Andó, S., France-Lanord, C., Vezzoli, G., Najman, Y., 2010. Mineralogical and chemical variability of fluvial sediments. 1. Bedload sand (Ganga–Brahmaputra, Bangladesh). Earth Planet. Sci. Lett. 299, 368–381.
- Garzanti, E., Andó, S., France-Lanord, C., Galy, V., Censi, P., Vignola, P., 2011. Mineralogical and chemical variability of fluvial sediments. 2. Suspended-load silt (Ganga–Brahmaputra, Bangladesh). Earth Planet. Sci. Lett. 302, 107–120.
- Garzanti, E., Resentini, A., Vezzoli, G., Andó, S., Malusà, M., Padoan, M., 2012. Forward compositional modelling of alpine orogenic sediments. Sediment. Geol. 280,149–164.
- Garzanti, E., Limonta, M., Resentini, A., Bandopadhyay, P.C., Najman, Y., Andó, S., Vezzoli, G., 2013a. Sediment recycling at convergent plate margins (Indo-Burman ranges and Andaman–Nicobar ridge). Earth Sci. Rev. 123, 113–132.
- Garzanti, E., Padoan, M., Andó, S., Resentini, A., Vezzoli, G., Lustrino, M., 2013b. Weathering and relative durability of detrital minerals in equatorial climate: sand petrology and geochemistry in the East African Rift. J. Geol. 121, 547–580.
- Garzanti, E., Vermeesch, P., Padoan, M., Resentini, A., Vezzoli, G., Andó, S., 2014. Provenance of passive-margin sand (southern Africa). J. Geol. 122, 17–42.

- Garzanti, E., Andó, S., Padoan, M., Vezzoli, G., El Kammar, A., 2015a. The modern Nile sediment system: processes and products. Quat. Sci. Rev. 130, 9–56.
- Garzanti, E., Resentini, A., Andó, S., Vezzoli, G., Vermeesch, P., 2015b. Physical controls on sand composition and relative durability of detrital minerals during long-distance littoral and eolian transport (coastal Namibia). Sedimentology 62, 971–996.
- Griffin, W.L., Powell, W.J., Pearson, N.J., O'Reilly, S.Y., 2008. GLITTER: data reduction soft- ware for laser ablation ICP–MS. In: Sylvester, P. (Ed.), Laser Ablation–ICP–MS in the Earth Sciences: Current Practices and Outstanding Issues. Mineralogical Association of Canada Short Course Vol. 40, pp. 308–311.
- Gururajan, N.S., Choudhuri, B.K., 2003. Geology and tectonic history of the Lohit valley, eastern Arunachal Pradesh, India. J. Asian Earth Sci. 21, 731–741.
- Hay, W.W., 1998. Detrital sediment fluxes from continents to oceans. Chem. Geol. 145, 287–323.
- Hinderer, M., 2012. From gullies to mountain belts: a review of sediment budgets at various scales. Sediment. Geol. 280, 21–59.
- Hubert, J.F., 1962. A zircon-tourmaline-rutile maturity index and the interdependence of the composition of heavy minerals assemblages with the gross composition and texture of sandstones. J. Sediment. Petrol. 32, 440–450.
- Hu, Z., Gao, S., 2008. Upper crustal abundances of trace elements: a revision and update. Chem. Geol. 253, 205–221.
- Ingersoll, R.V., Bullard, T.F., Ford, R.L., Grimm, J.P., Pickle, J.D., Sares, S.W., 1984. The effect of grain size on detrital modes: a test of the Gazzi–Dickinson point-counting method. J. Sediment. Petrol. 54, 103–116.
- Kirby, E., Whipple, K.X., 2012. Expression of active tectonics in erosional landscapes. J. Struct. Geol. 44, 54–75.
- Kirby, E., Whipple, K.X., Tang, W., Chen, Z., 2003. Distribution of active rock uplift along the eastern margin of the Tibetan plateau: inferences from bedrock channel longitudinal profiles. J. Geophys. Res. 108 (B4), 2217. http://dx.doi.org/10.1029/ 2001JB000861.
- Korup, O., Schlunegger, F., 2009. Rock-type control on erosion-induced uplift, eastern Swiss alps. Earth Planet. Sci. Lett. 278, 278–285.
- Li, C., Yang, S., 2010. Is chemical index of alteration (CIA) a reliable proxy for chemical weathering in global drainage basins? Am. J. Sci. 310, 111–127.
- Liang, Y.-H., Chung, S.-L., Liu, D., Xu, Y., Wu, F.-Y., Yang, J.-H., Wang, Y., Lo, C.-H., 2013. Detrital zircon evidence from Burma for reorganization of the eastern Himalayan river system. Am. J. Sci. 308, 618–638.
- Licht, A., Reisberg, L., France-Lanord, C., Soe, A.N., Jaeger, J.J., 2016. Cenozoic evolution of the central Myanmar drainage system: insights from sediment provenance in the Minbu sub-basin. Basin Res. 28, 237–251.

- Limonta, M., Resentini, A., Carter, A., Bandopadhyay, P.C., Garzanti, E., 2016. Provenance of Oligocene Andaman Sandstones (Andaman–Nicobar islands): Ganga–Brahmaputra or Irrawaddy derived? Geological Society London, Special Publication
- Lin, T.-H., Chung, S.-L., Kumar, A., Wu, F.-Y., Chiu, H.-Y., Lin, I., 2013. Linking a prolonged Neo-Tethyan magmatic arc in south Asia: zircon U-Pb and Hf isotopic constraints from the Lohit Batholith, NE India. Terra Nova 25, 453–458.
- Lupker, M., France-Lanord, C., Lavé, J., Bouchez, J., Galy, V., Métivier, F., Gaillardet, J., Lartiges, B., Mugnier, J.L., 2011. A Rouse-based method to integrate the chemical composition of river sediments: application to the Ganga basin. J. Geophys. Res. 116, F04012. http://dx.doi.org/10.1029/2010JF001947.
- Lupker, M., France-Lanord, C., Galy, V., Lavé, J., Gaillardet, J., Gajurel, A.P., Guilmette, C., Rahman, M., Singh, S.K., Sinha, R., 2012. Predominant floodplain over mountain weathering of Himalayan sediments (Ganga basin). Geochim. Cosmochim. Acta 84, 410–432.
- Malusà, M.G., Resentini, A., Garzanti, E., 2015. Hydraulic sorting and mineral fertility bias in detrital geochronology. Gondwana Res. 31, 1–19.
- McDonough, W.F., Sun, S.S., 1995. The composition of the earth. Chem. Geol. 120, 223–253.
- Mitchell, A.H.G., Htay, M.T., Htun, K.M., Win, M.N., Oo, T., Hlaing, T., 2007. Rock relationships in the Mogok metamorphic belt, Tatkon to Mandalay, central Myanmar. J. Asian Earth Sci. 29, 891–910.
- Mitchell, A., Chung, S.L., Oo, T., Lin, T.H., Hung, C.H., 2012. Zircon U-Pb ages in Myanmar: magmatic–metamorphic events and the closure of a neo-Tethys ocean? J. Asian Earth Sci. 56, 1–23.
- Nesbitt, H.W., Young, G.M., 1982. Early Proterozoic climates and plate motions inferred from major element chemistry of lutites. Nature 299, 715–717.
- Nie, J., Stevens, T., Rittner, M., Stockli, D., Garzanti, E., Limonta, M., Bird, A., Andò, S., Vermeesch, P., Saylor, J., Lu, H., Breecker, D., Hu, X., Liu, S., Resentini, A., Vezzoli, G., Peng, W., Carter, A., Ji, S., Pan, B., 2015. Loess plateau storage of northeastern Tibetan plateau-derived Yellow River sediment. Nat. Commun. 6 http://dx.doi.org/10.1038/ncomms9511.
- Oo, K.-L., Zaw, K., Meffre, S., Aung, D.-W., Lai, C.-K., 2015. Provenance of the Eocene sand- stones in the southern Chindwin basin, Myanmar: implications for the unroofing his- tory of the Cretaceous–Eocene magmatic arc. J. Asian Earth Sci. 107, 172–194.
- Ouimet, W.B., Whipple, K.X., Granger, D.E., 2009. Beyond threshold hillslopes: channel ad- justment to base-level fall in tectonically active mountain ranges. Geology 37, 579–582.
- Padoan, M., Garzanti, E., Harlavan, Y., Villa, I.M., 2011. Tracing Nile sediment sources by

Sr and Nd isotope signatures (Uganda, Ethiopia, Sudan). Geochim. Cosmochim. Acta 75, 3627–3644.

- Parker, A., 1970. An index of weathering for silicate rocks. Geol. Mag. 107, 501–504.
- Ra, K., 2011. Water quality management at river basin in Myanmar, 3rd WEPA Internation Workshop, Manila 14 pp.
- Robinson, R.A.J., Bird, M.I., Oo, N.W., Hoey, T.B., Aye, M.M., Higgitt, D.L., Lu, X.X., Swe, A., Tun, T., Win, S.L., 2007. The Irrawaddy River sediment flux to the Indian Ocean: the original nineteenth-century data revisited. J. Geol. 115, 629–640.
- Robinson, R.A., Brezina, C.A., Parrish, R.R., Horstwood, M.S., Oo, N.W., Bird, M.I., Thein, M., Walters, A.S., Oliver, G.J.H., Zaw, K., 2014. Large rivers and orogens: the evolution of the Yarlung Tsangpo–Irrawaddy system and the eastern Himalayan syntaxis. Gondwana Res. 26, 112–121.
- Rubey, W.W., 1933. The size-distribution of heavy minerals within a water-laid sandstone. J. Sediment. Petrol. 3, 3–29.
- Rudnick, R.L., Gao, S., 2003. Composition of the continental crust. In: Rudnick, R.L., Holland, H.D., Turekian, K.K. (Eds.), Treatise on GeochemistryThe Crust Vol. 3. Elsevier Pergamon, Oxford, pp. 1–64.
- Russell, R.D., 1937. Mineral composition of Mississippi river sands. Geol. Soc. Am. Bull. 48, 1307–1348.
- Searle, M.P., Noble, S.R., Cottle, J.M., Waters, D.J., Mitchell, A.H.G., Hlaing, T., Horstwood, M.S.A., 2007. Tectonic evolution of the Mogok metamorphic belt, Burma (Myanmar) constrained by U-Th-Pb dating of metamorphic and magmatic rocks. Tectonics 26, TC3014. http://dx.doi.org/10.1029/2006TC002083.
- Sevastjanova, I., Hall, R., Rittner, M., Paw, S.M.T.L., Naing, T.T., Alderton, D.H., Comfort, G., 2016. Myanmar and Asia united, Australia left behind long ago. Gondwana Res. 32, 26–40.
- Shahzad, F., Gloaguen, R., 2011. TecDEM: a MATLAB based toolbox for tectonic geomorphology, part 1: drainage network pre-processing and stream profile analysis. Comput. Geosci. 37, 250–260.
- Shao, J., Yang, S., Li, C., 2012. Chemical indices (CIA and WIP) as proxies for integrated chemical weathering in China: inferences from analysis of fluvial sediments. Sedi- ment. Geol. 265, 110–120.
- Shi, G., Lei, W., He, H., Ng, Y.-N., Liu, Y., Liu, Y., Yuan, Y.-X., Kang, Z., Xie, G., 2014. Superimposed tectono-metamorphic episodes of Jurassic and Eocene age in the jadeite uplift, Myanmar, as revealed by 40Ar/39Ar dating. Gondwana Res. 26, 464–474.
- Singh, S.K., France-Lanord, C., 2002. Tracing the distribution of erosion in the Brahmaputra watershed from isotopic compositions of stream sediments. Earth Planet. Sci. Lett. 202, 645–662.

- Stamp, L.D., 1940. The Irrawaddy river. Geogr. J. 95, 329–352.
- Stephenson, D., Marshall, T.R., 1984. The petrology and mineralogy of Mt. Popa Volcano and the nature of the late-Cenozoic Burma volcanic arc. J. Geol. Soc. Lond. 141, 747–762.
- Syvitski, J.P., Kettner, A., 2011. Sediment flux and the anthropocene. Philos. Trans. R. Soc. Lond. A Math. Phys. Eng. Sci. 369, 957–975.
- Vermeesch, P., Resentini, A., Garzanti, E., 2016. An R package for statistical provenance analysis. Sediment. Geol. 336, 14–25.
- Vezzoli, G., Garzanti, E., Vincent, S.J., Andó, S., Carter, A., Resentini, A., 2014. Tracking sediment provenance and erosional evolution of the western Greater Caucasus. Earth Surf. Process. Land. 39, 1101–1114.
- Vezzoli, G., Garzanti, E., Limonta, M., Andó, S., Yang, S., 2016. Erosion patterns in the Changjiang (Yangtze river) catchment revealed by bulk-sample versus single-mineral provenance budgets. Geomorphology 261, 177–192.
- von Blanckenburg, F., 2005. The control mechanisms of erosion and weathering at basin scale from cosmogenic nuclides in river sediment. Earth Planet. Sci. Lett. 237, 462–479.
- von Eynatten, H., Dunkl, I., 2012. Assessing the sediment factory: the role of single grain analysis. Earth Sci. Rev. 115, 97–120.
- Wang, J.-G., Wu, F.-Y., Tan, X.-C., Liu, C.-Z., 2014. Magmatic evolution of the western Myanmar arc documented by U-Pb and Hf isotopes in detrital zircon. Tectonophysics 612, 97–105.
- Win, S.H., 2011. Sediment Dynamics in Irrawaddy River, Myanmar. Master of Social Science Thesis, National University of Singapore 265 pp.
- Whipple, K.X., Tucker, G.E., 1999. Dynamics of the stream-power river incision model: implications for height limits of mountain ranges, landscape response timescales, and research needs. J. Geophys. Res. 104, 17661–17674.
- Whipple, K.X., 2004. Bedrock rivers and the geomorphology of active orogens. Annu. Rev. Earth Planet. Sci. 32, 151–185.
- Willett, S.D., McCoy, S.W., Perron, J.T., Goren, L., Chen, C.Y., 2014. Dynamic reorganization of river basins. Science 343, 1248765.
- Xie, L.W., Zhang, Y.B., Zhang, H.H., Sun, J.F., Wu, F.Y., 2008. In situ simultaneous determination of trace elements, U-Pb and Lu-Hf isotopes in zircon and baddeleyite. Chin. Sci.Bull. 53, 1565–1573.
- Yang, S., Jung, H.S., Lia, C., 2004. Two unique weathering regimes in the Changjiang and Huanghe drainage basins: geochemical evidence from river sediments. Sediment. Geol. 164, 19–34.
- Zhao, S.W., Lai, S.C., Qin, J.F., Zhu, R.Z., 2016. Tectono-magmatic evolution of the Gaoligong belt, southeastern margin of the Tibetan plateau: constraints from granitic gneisses and granitoid intrusions. Gondwana Res.

http://dx.doi.org/10.1016j.gr.2015.05.007.

- Zin, W.W., Nestmann, F., Ihringer, J., 2009. Flood forecasting using FGM model in Chindwin river basin. Malays. J. Civ. Eng. 21, 135–151.

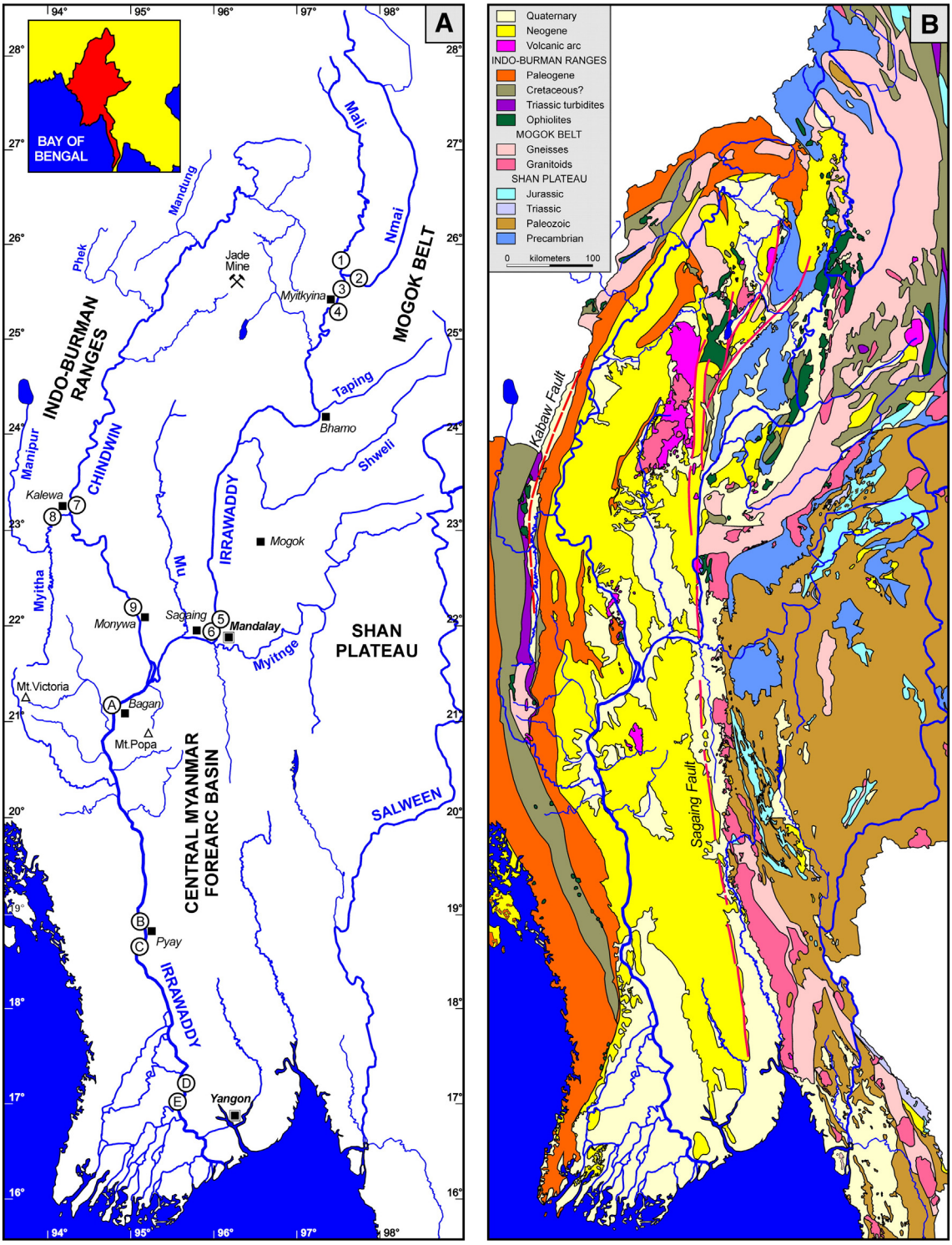

Fig. 1. Location and geology of the Irrawaddy (Ayeyarwadi) River basin. A) Sampling sites (full information provided in Appendix Table S1 and Google Earth file Irrawaddy.kml). B) Geology of the region after the Geological Map of Myanmar (1977; scale 1:1,500,000).

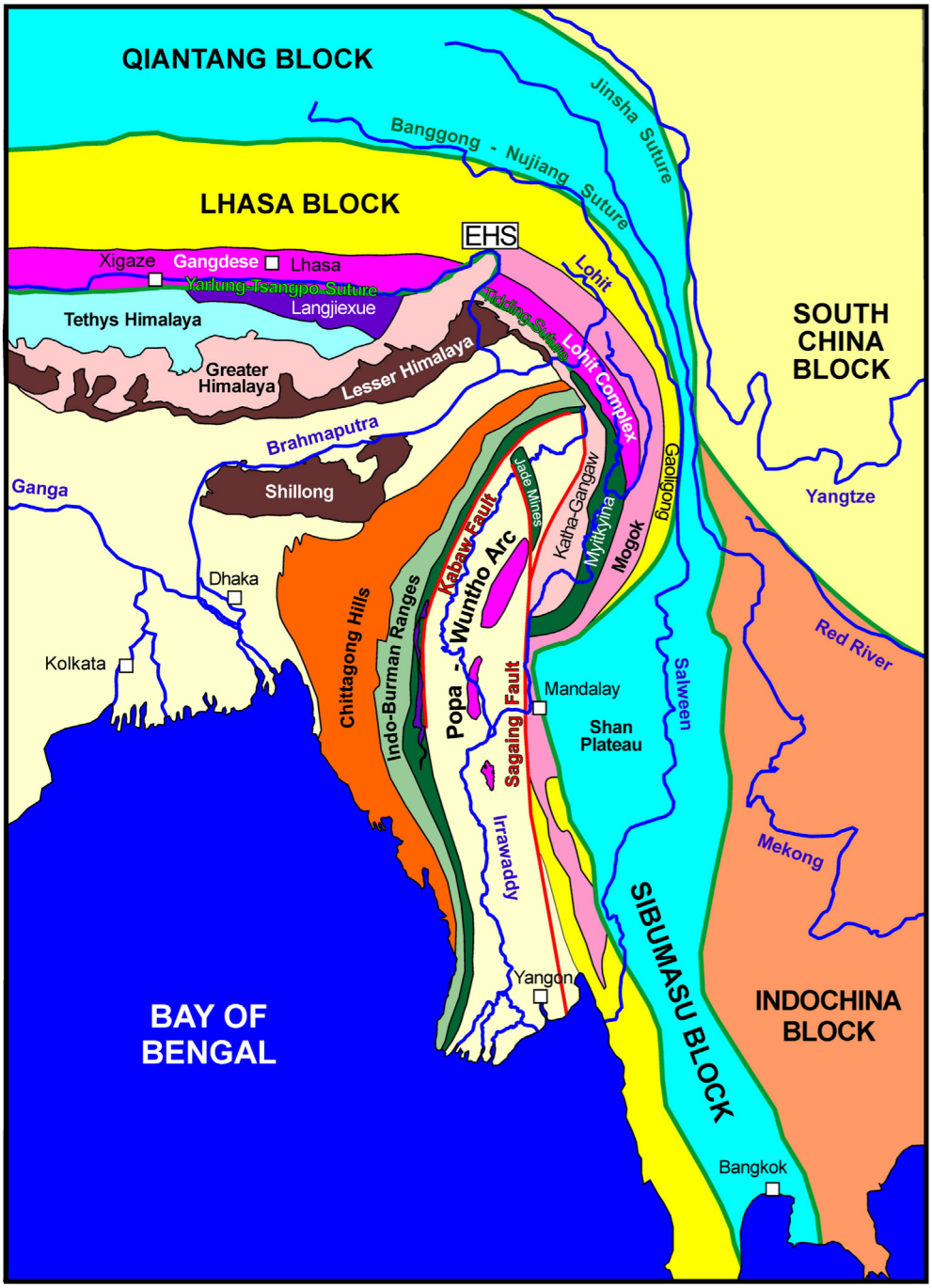

Fig. 2. Tectonic sketch map showing correlation of geological domains, suture zones and magmatic arcs around the Eastern Himalayan Syntaxis (EHS; modified after Mitchell et al., 2012).

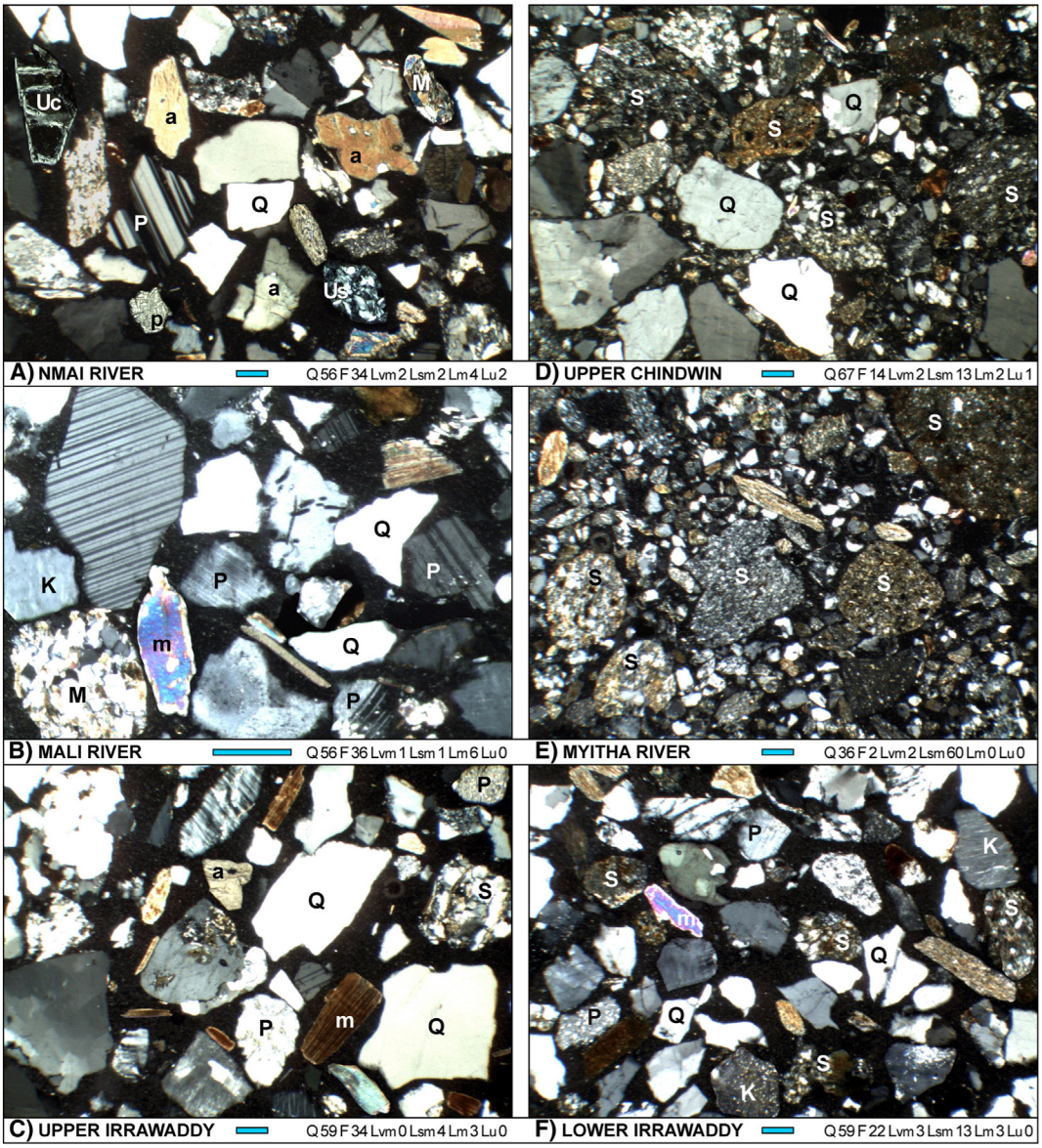

Fig. 3. Petrographic signatures of Irrawaddy sands. The Nmai (A) and Mali Rivers (B) chiefly drain the Mogok Belt and Lohit Plutonic Complex (Fig. 2) and carry abundant feldspars (K = K- feldspar; P = plagioclase), high-rank metamorphic rock fragments (M) and micas (m). Heavy minerals (a = amphibole; p = pyroxene) are abundant in Nmai sand, which includes ophiolite-derived cellular (Uc) and schistose (Us) serpentinite grains. C) Irrawaddy sand at Mandalay is slightly enriched in quartz (Q) and sedimentary rocks fragments (S) supplied by left-bank tributaries draining the Shan Plateau. D) Feldspatho-litho-quartzose upper Chindwin sand is rich in terrigenous rocks fragments (S) derived from the Indo-Burman Ranges and dominant in Myitha sand (E). F) Irrawaddy sand reaching the Andaman Sea is rich both in feldspars largely derived from Nmai and Mali headwaters and in sedimentary to low-rank metasedimentary rock fragments largely contributed by the Chindwin River. Q = quartz; F = feldspars; L = lithic fragments (Lvm = volcanic to low-rank metavolcanic; Lsm = sedimentary to low-rank metasedimentary; Lm = high-rank metamorphic; Lu = ultramafic). Blue bar = 250 μm.

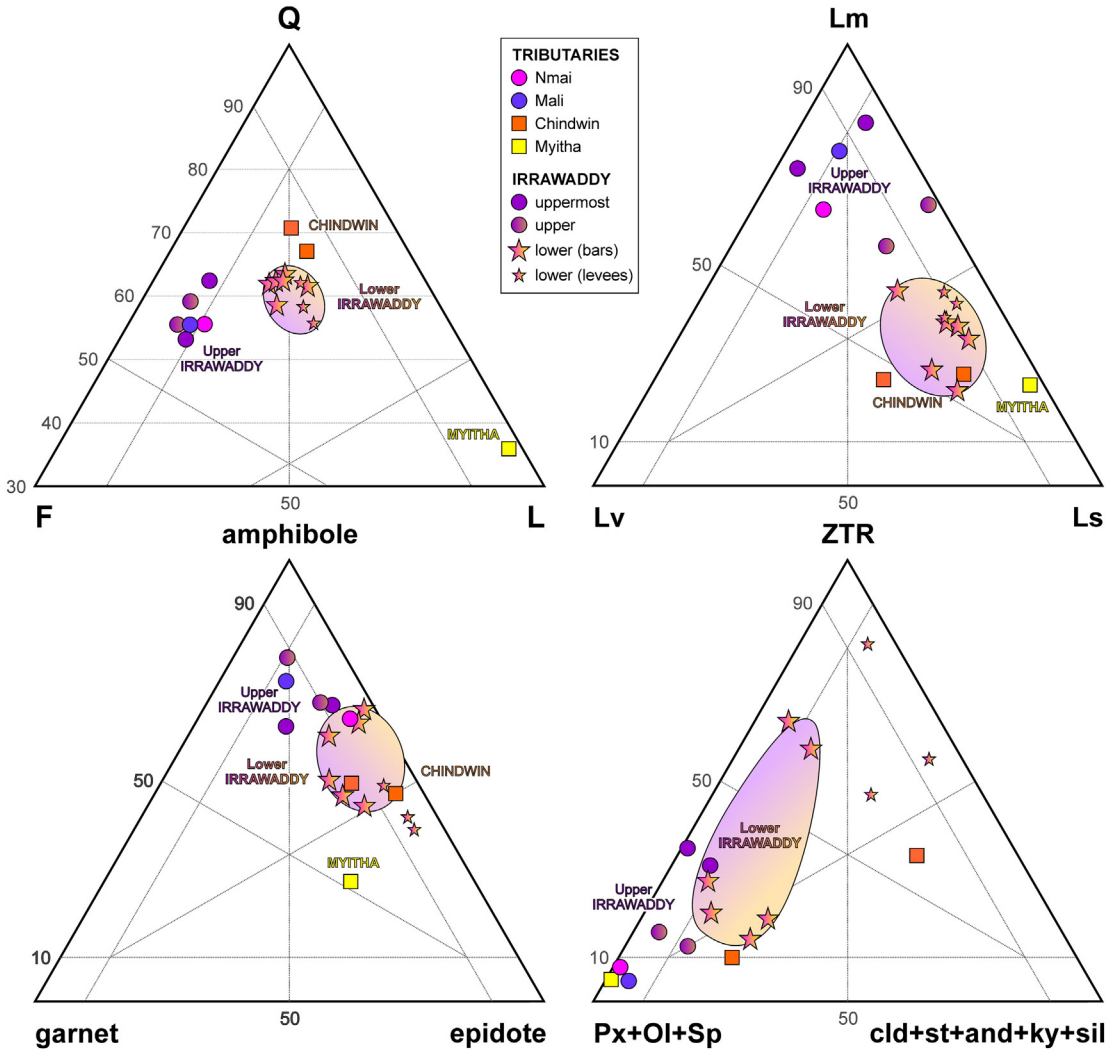

Fig. 4. Petrography and heavy minerals in the Irrawaddy basin. Irrawaddy sand is a mixture of high-rank metamorphiclastic to plutoniclastic detritus supplied by the Nmai and Mali headwater branches and very-low-rank sedimentaclastic/metasedimentaclastic detritus largely derived from the Indo-Burman Ranges via the Chindwin River. Ophiolitic detritus occurs in the Nmai and Myitha Rivers, whereas volcanic detritus from arc-related rocks appears in the lower Chindwin and lower Irrawaddy. Detritus from cover rocks of the Shan Plateau is subordinate. Q = quartz; F = feldspars; L = lithic fragments (Lv = volcanic; Ls = sedimentary; Lm = metamorphic). ZTR = zircon + tourmaline + rutile; Px = pyroxene; Ol = olivine; Sp = Cr-spinel; Cld = chloritoid; st = staurolite; and =andalusite; ky = kyanite; Sil = sillimanite.

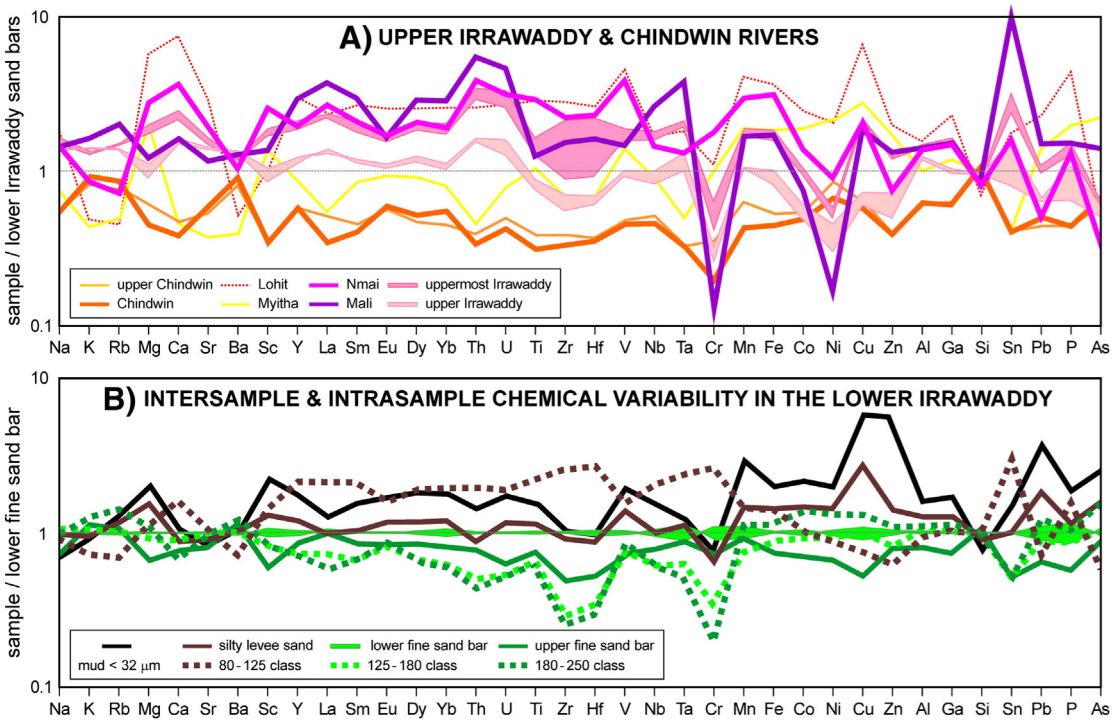

Fig. 5. Chemistry of Irrawaddy sediments (elements arranged following the periodic table group by group). A) Compositional trends chiefly reflect progressive downstream increase in recycled detritus (concentrations normalized to averaged analyses of 7 lower Irrawaddy sand bars). Geochemistry of Nmai sand reflects abundance of mafic minerals and is similar to that of Lohit River sand (data from Singh and France-Lanord, 2002), characterized by lower quartz/feldspar ratio and even higher heavy-mineral concentration (Garzanti et al., 2004). Concentration of most chemical elements decreases from Myitkyina (uppermost Irrawaddy; localities 3 and 4 in Fig. 1A) to Mandalay and Sagaing (upper Irrawaddy; localities 5 and 6 in Fig. 1A), suggesting supply from left-bank tributaries of detritus recycled from cover strata of the Shan Plateau. Depletion of most elements caused by sediment recycling and quartz dilution is most evident for Chindwin sand, showing minor changes from upstream (upper Chindwin) to downstream of the Myitha confluence. B) In the absence of significant selective-entrainments effects, intersample variability is not more than intrasample variability controlled by the settling-equivalence effect (mud, silty levee and sand bar samples all collected at site E in Fig. 1A; concentrations normalized to averaged replicate analyses of sample 3200FS). Most elements are more abundant in mud than in silty levees, and in silty levees than in sands; only Si, K and Ba, largely hosted in quartz and K-feldspar, are more abundant in coarser sand bars. Elements principally hosted in heavy minerals (e.g., REE, Ti, Zr, Hf, Nb, Ta, Cr) concentrate systematically in the fine tail of the size distribution, whereas elements preferentially hosted in micas (e.g., K, Rb, Ba) concentrate in the coarse tail.

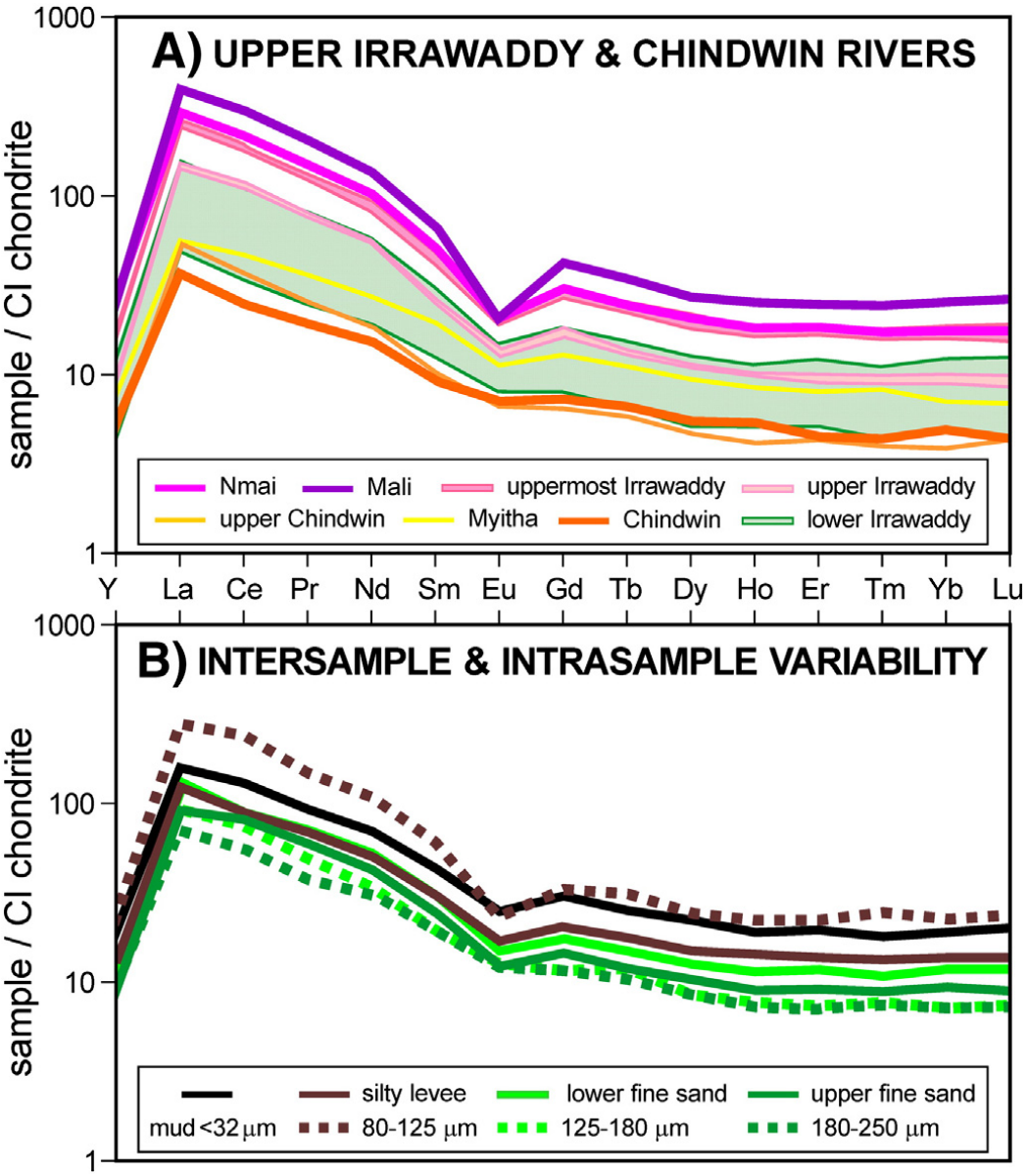

Fig. 6. Chondrite-normalized YREE patterns of all Irrawaddy sediments display classical LREE enrichment, negative Eu anomaly, and flat HREE distribution. A) The strongly negative Eu anomaly in Mali sand reflects occurrence of allanite, derived from granitoid rocks and traced downstream as far as the delta. YREE patterns of Nmai and uppermost Irrawaddy sands are virtually identical. Chindwin sand is low in REE, and thus REE concentration decreases downstream of the Chindwin confluence. B) REE content increases progressively with decreasing grain size.

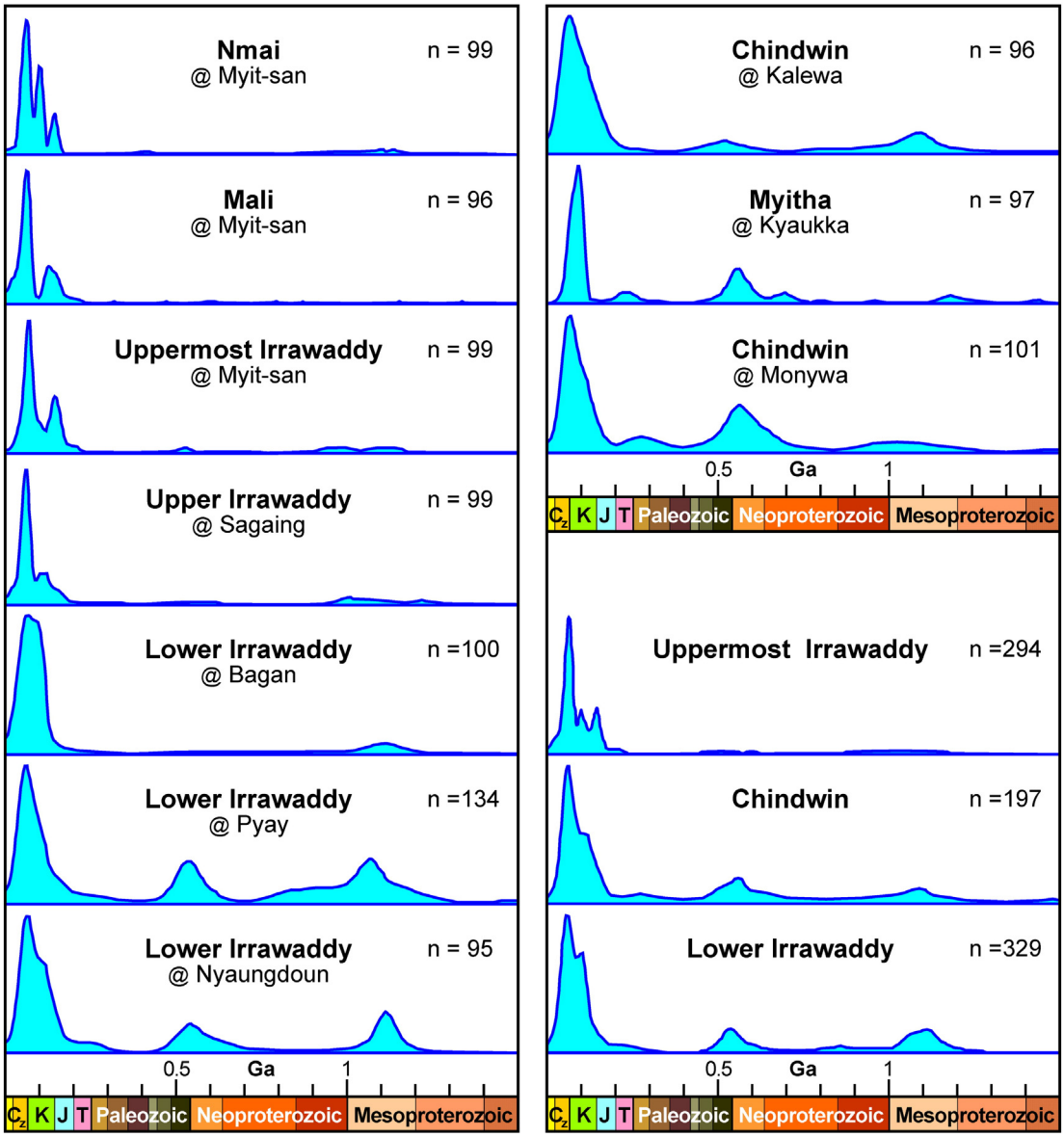

Fig. 7. U\Pb age spectra of detrital zircons in Irrawaddy river sands (age vs. frequencies plotted as Kernel Density Estimates using software package Provenance; Vermeesch et al., 2016). Left panel: Detrital zircons of dominantly Miocene to Jurassic ages in Irrawaddy headwaters mix progressively downstream with pre-Mesozoic zircons largely recycled from sedimentary units. Pyay sample analysed by Andrew Carter (University College London). Right panel (above): discernible zircon supply from the Myitha tributary to Chindwin sand. Right panel (below): age distribution in lower Irrawaddy sand is intermediate between Chindwin and upper Irrawaddy age spectra. We used 206Pb/238U and 207Pb/206Pb ages for zircons younger and older than 1000 Ma, respectively; n = number of concordant ages.

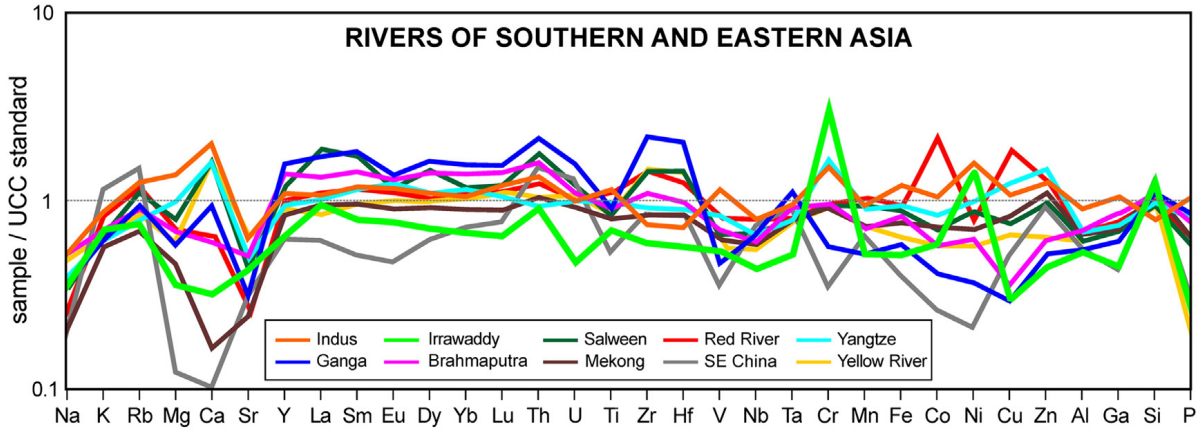

Fig. 8. Large Asian rivers sourced in Himalayan or Tibetan highlands efficiently mediate provenance signals from different parts of the huge watershed and thus carry sand-sized sediments with composition broadly similar to the estimated average value for the upper continental crust. Irrawaddy sand is depleted in most elements relative to the UCC standard because of extensive recycling of siliciclastic units especially in the Chindwin catchment, and yet it shows the highest concentration in Cr and one of the highest in Ni, reflecting contribution from suture-zone ophiolites and volcanic arcs. Indus, Salween, Yangtze and Yellow River sands are Ca-rich because they include significant carbonate rock fragments, whereas Brahmaputra, Irrawaddy, Mekong, Red River and SE China rivers (Oujiang, Minjiang, Mulanxi, Jiulongjiang, and Hanjiang) carry little or no carbonate grains. Data are after Singh and France-Lanord (2002); Galy et al. (2007); Borges et al. (2008); Clift et al. (2010); Garzanti et al. (2010); Lupker et al. (2011, 2012), and include analyses on Mekong and Yangtze sands kindly provided by Shouye Yang (Tongji University) and own unpublished analyses of SE China river sands.

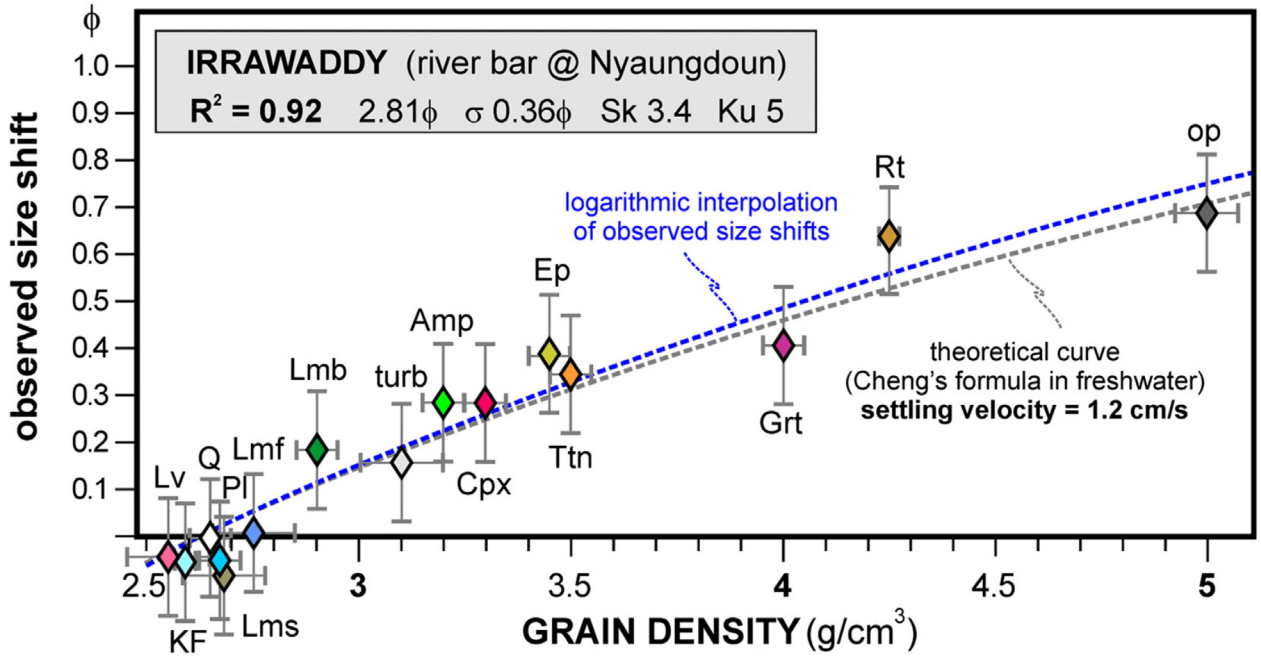

Fig. 9. Settling-equivalence analysis of Irrawaddy bar sand (sample 3200FS; multiple-window method at 0.5 φ interval) indicates that 92% of intrasample mineralogical variability is accounted for by size-density sorting. The size shift is the difference in size between a given mineral and quartz in φ units (see Garzanti et al., 2008 for more methodological information). Mineral abbreviations: Amp = amphibole; Cpx = clinopyroxene; Ep = epidote; Grt = garnet; KF = K-feldspar; L = lithic grains (Lv = volcanic; Lms = low-rank metasedimentary; Lmf = felsic metamorphic; Lmb = metabasite); op = opaque Fe\Ti\Cr oxides; Pl = plagioclase; Q = quartz; Rt = rutile; Ttn = titanite; turb = turbid minerals.

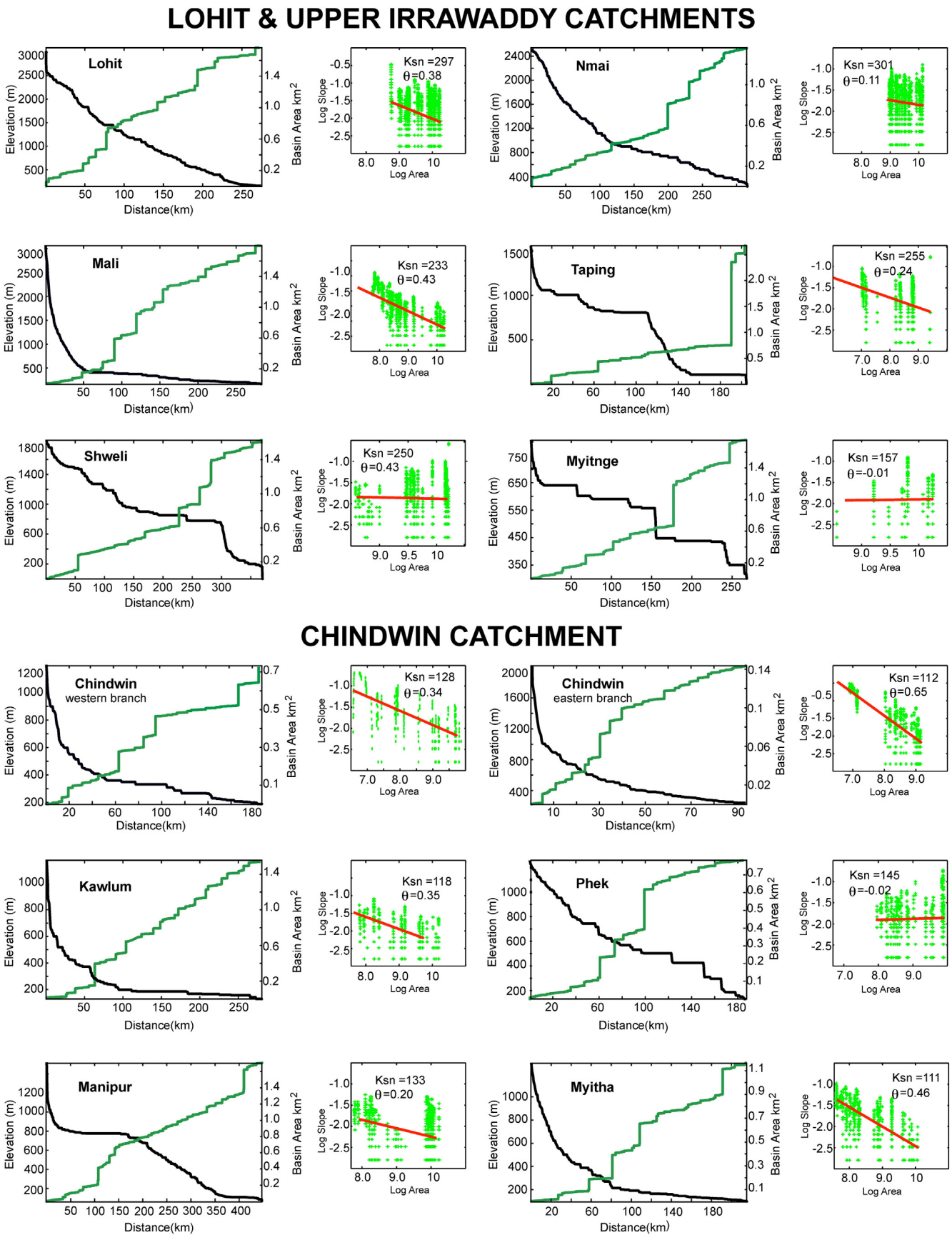

Fig. 10. Geomorphological analysis of the studied Irrawaddy tributaries, showing area (green line), longitudinal river profile (black line) and slope-area data for each. (For interpretation of the references to colour in this figure legend, the reader is referred to the web version of this article.)

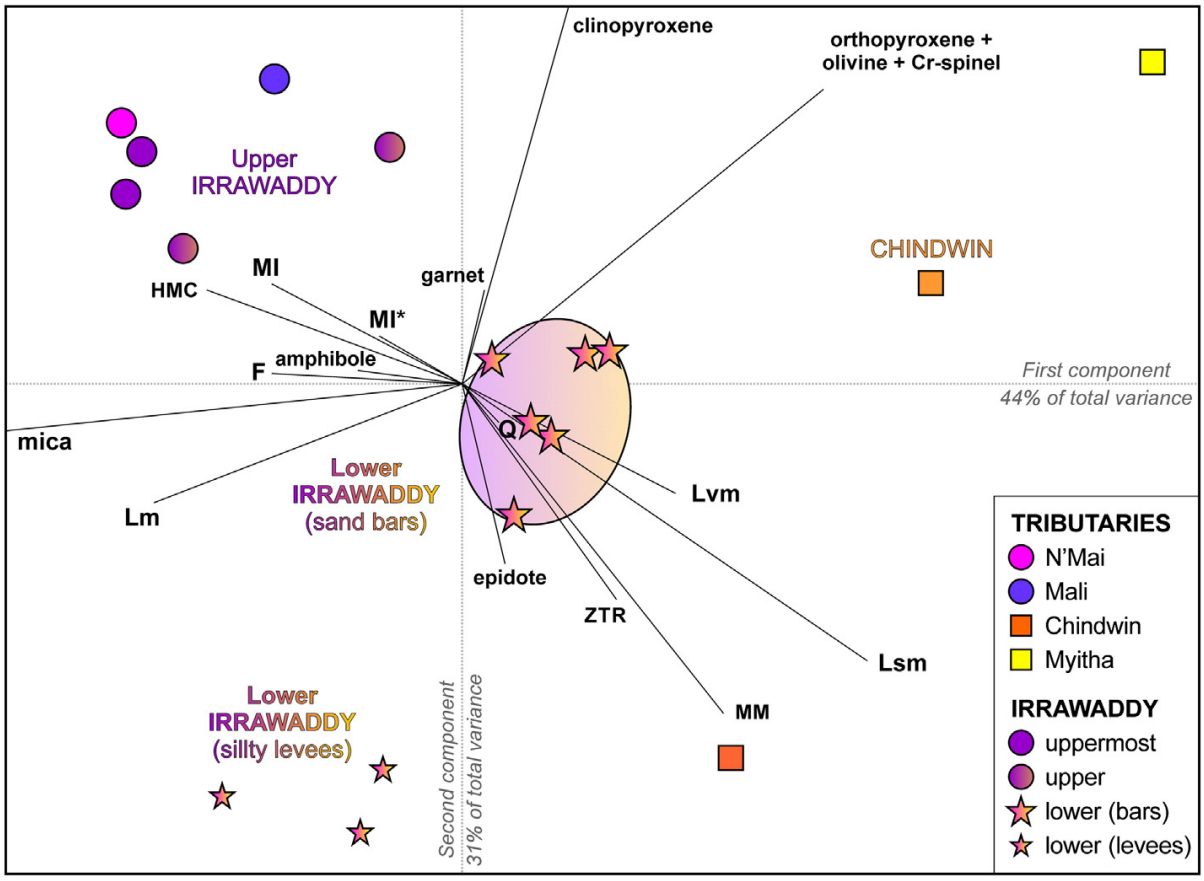

Fig. 11. Provenance of Irrawaddy sediments discriminated with compositional biplot (Gabriel, 1971). Upper Irrawaddy sands are derived in subequal proportions from the Nmai and Mali headwater branches, with progressive downstream addition of detritus supplied by left-bank tributaries draining largely sedimentary rocks of the Shan Plateau. Lower Irrawaddy sands are instead markedly enriched in quartz and sedimentary to low-rank metasedimentary rock fragments supplied by the Chindwin River and its tributaries draining the Indo-Burman Ranges. Both multivariate observations (points) and variables (rays) are displayed. The length of each ray is proportional to the variability of the compositional parameter in the data set. If the angle between two rays is close to 0°, 90°, or 180°, then the corresponding parameters are directly correlated, uncorrelated, or inversely correlated, respectively.

#	River	Site	Facies	GSZ	Q	F	Lvm	Lsm	Lm	Lu	mica	HM	total	P/F	MI*	MI	tHMC	SRD	ZTR	Ttn	Ap	Ep	Grt	MM	Amp	Px	Ol	Sp	&tHM	Total
1	Nmai Hka	Myit-san	Bar	280	46	28	2	2	4	2	4	14	100.0	64	341	295	14	2.82	0.5	0	0.5	12	13	0.5	65	8	1	0	0	100.0
2	Mali Hka	Myit-san	Bar	200	50	32	1	1	5	0	6	5	100.0	53	358	332	3	2.72	0.5	6	0.5	26	5	0	55	6	0.5	0	0	100.0
3	Irrawaddy	Myit-san	Bar	235	49	23	2	0	4	0	8	13	100.0	59	354	304	9	2.76	2	1	0	23	7	0.5	62	3	0	0.5	0	100.0
4	Irrawaddy	Myitkyina	Bar	170	43	30	0	2	5	1	9	11	100.0	58	335	326	8	2.78	3	1	0.5	17	17	0	56	3	1	1	0	100.0
5	Irrawaddy	Mandalay	Bar	230	51	29	0	3	2	0	6	9	100.0	64	310	266	6	2.72	0.4	0.4	0.4	22	9	0.4	65	2	0	0.4	0	100.0
6	Irrawaddy	Sagaing	Bar	270	52	35	1	3	2	0	1	6	100.0	51	307	252	4	2.69	1	1	0	10	10	0.5	69	7	0	0	0	100.0
7	Chindwin	Kalewa	Bar	360	66	14	2	13	2	1	0	2	100.0	49	226	81	2	2.65	3	0	0.5	42	5	5	42	0	0	2	0	100.0
8	Myitha	Kyaukka	Bar	350	35	2	2	59	0	0	0	1	100.0	57	114	49	0.4	2.59	4	0	0.9	18	9	0.5	10	55	0	3	0	100.0
9	Chindwin	Monywa	Bar	320	70	15	5	8	1	0	0	1	100.0	50	172	85	0.4	2.64	2	1	0.5	30	10	4	39	12	0.5	1	0	100.0
A	Irrawaddy	Bagan	Bar	330	59	18	3	10	3	0	4	3	100.0	58	224	127	2	2.67	1	0.9	0.5	25	11	2	54	6	0	0	0	100.0
B	Irrawaddy	Pyay	Levee	120	49	17	2	16	4	1	8	4	100.0	62	179	127	2	2.69	4	1	2	39	6	3	43	0.4	0	1	0	100.0
B	Irrawaddy	Pyay	Bar	215	58	16	5	13	3	0	3	3	100.0	49	212	86	3	2.68	10	0.5	0.5	31	14	1	39	3	0.5	1	1	100.0
C	Irrawaddy	Shwedaung	Levee	90	55	15	2	13	3	1	7	4	100.0	73	184	117	3	2.69	5	1	2	46	5	4	37	0	0	0.5	0	100.0
C	Irrawaddy	Shwedaung	Bar	225	61	19	2	12	3	0	1	2	100.0	57	243	130	3	2.68	3	4	0.8	38	12	0.8	40	1	0.4	0	0	100.0
D1	Irrawaddy	Nyaungdoun	Bar	240	60	20	4	9	3	1	2	1	100.0	47	172	117	1	2.66	1	1	0	29	2	2	60	4	0	0	0.5	100.0
D2	Irrawaddy	Nyaungdoun	Bar	190	60	21	2	12	1	0	0	3	100.0	53	160	94	3	2.66	1	1	0	30	5	0.5	59	3	0	0.5	0.0	100.0
E	Irrawaddy	Nyaungdoun	Levee	100	52	17	2	14	4	1	6	4	100.0	61	196	125	2	2.68	3	0.5	0.5	53	6	0.5	37	0	0	0	0	100.0
E	Irrawaddy	Nyaungdoun	Finer bar	80–125	52	14	6	13	4	0	2	10	100.0	51	208	104	8	2.74	2	3	1	42	6	2	40	1	0	1	1	100.0
E	Irrawaddy	Nyaungdoun	Finer bar	125–180	46	24	9	16	3	0	2	1	100.0	50	192	116	1	2.65	0.5	3	0	33	7	0	51	5	0	0	0.5	100.0
E	Irrawaddy	Nyaungdoun	Finer bar	180–250	45	22	7	15	2	0	8	0	100.0	54	174	86	0.4	2.66	0	3	0	33	2	0	56	5	0	0	0.9	100.0
E	Irrawaddy	Nyaungdoun	Coarser bar	220	57	22	3	12	3	0	1	2	100.0	47	240	65	2	2.65	1	2	0.5	30	15	1	45	5	0	0	0	100.0

Table 1. Key petrographic and mineralogical parameters of Irrawaddy sand bars and silty levee sands. QFL parameters as in Fig. 3; GSZ = grain size; HM = heavy minerals. MI* and MI = metamorphic indices. tHMC = transparent heavy-mineral concen- tration. SRD = Source Rock Density index (i.e., estimated grain density in g/cm3). ZTR = zircon + tourmaline + rutile; Ttn = titanite; Ap = apatite; Ep = epidote; Grt = garnet; MM = chloritoid + staurolite + andalusite + kyanite + sillimanite; Amp = amphibole; Px = pyroxene; Ol = olivine; Sp = Cr-spinel; &tHM = other transparent heavy minerals (Ti oxides, monazite). Full datasets provided in Appendix Tables A2 and A3.

#	River	Site	Deposit	SiO_2	Al_2O_3	Fe_2O_3	MgO	CaO	Na_2O	K_2O	TiO_2	P_2O_5	MnO	LOI	Rb	Sr	Ba	Sc	Y
			(class)	wt%	wt%	wt%	wt%	wt%	wt%	wt%	wt%	wt%	wt%	wt%	ppm	ppm	ppm	ppm	ppm
1	Nmai Hka	Myit-san	Sand bar	65.5	12.0	8.6	2.4	4.3	1.9	1.9	1.2	0.06	0.14	1.8	54	286	385	15	25
2	Mali Hka	Myit-san	Sand bar	71.9	12.2	4.7	1.1	1.9	1.9	3.6	0.5	0.07	0.08	2.0	153	170	479	8	38
3	Irrawaddy	Myit-san	Sand bar	71.8	12.2	4.3	1.6	2.6	2.0	2.9	0.5	0.06	0.08	1.9	113	216	449	10	24
4	Irrawaddy	Myitkyina	Sand bar	69.0	13.1	5.1	1.8	2.9	2.2	2.9	0.7	0.07	0.09	2.1	115	245	455	11	28
5	Irrawaddy	Mandalay	Sand bar	76.8	10.8	2.8	1.0	1.9	1.8	3.0	0.4	0.05	0.05	1.3	107	205	500	6	16
6	Irrawaddy	Sagaing	Sand bar	78.3	10.3	2.2	0.8	1.8	1.8	3.1	0.3	0.03	0.05	1.2	106	203	498	5	15
7	Chindwin	Kalewa	Sand bar	88.2	5.4	1.5	0.5	0.6	0.7	1.8	0.2	0.02	0.03	1.2	59	78	306	2	7
8	Myitha	Kyaukka	Sand bar	78.3	8.6	5.0	1.7	0.5	1.0	1.0	0.4	0.09	0.09	3.1	38	54	147	8	11
9	Chindwin	Monywa	Sand bar	87.7	5.4	1.2	0.4	0.5	0.7	2.0	0.1	0.02	0.02	1.9	66	84	343	2	8
A	Irrawaddy	Bagan	Sand bar	83.7	7.6	2.0	0.7	0.9	1.1	2.4	0.2	0.04	0.04	1.4	83	128	392	4	9
B	Irrawaddy	Pyay	Levee	71.3	12.2	4.6	1.7	1.3	1.6	2.0	0.6	0.08	0.07	4.5	85	159	361	10	21
B	Irrawaddy	Pyay	Sand bar	79.5	8.8	3.3	1.0	1.3	1.3	2.1	0.6	0.04	0.06	1.8	73	147	357	7	16
C	Irrawaddy	Shwedaung	Levee	73.4	11.6	4.2	1.5	1.4	1.7	1.9	0.6	0.08	0.06	3.3	77	170	335	9	20
C	Irrawaddy	Shwedaung	Sand bar	81.8	8.2	2.6	0.9	1.3	1.2	2.1	0.4	0.03	0.05	1.4	71	146	353	6	14
D1	Irrawaddy	Nyaungdoun	Sand bar	83.3	8.2	1.9	0.6	0.7	1.3	2.5	0.2	0.04	0.03	1.1	88	139	439	3	7
D2	Irrawaddy	Nyaungdoun	Sand bar	82.3	8.3	2.4	0.8	1.2	1.3	2.1	0.3	0.04	0.04	1.2	72	143	375	5	10
E	Irrawaddy	Nyaungdoun	Mud < 32 mm	58.8	16.3	7.2	2.3	1.5	1.1	1.9	0.9	0.14	0.16	9.4	96	138	347	19	30
E	Irrawaddy	Nyaungdoun	Levee	69.6	12.9	5.1	1.8	1.3	1.6	1.9	0.7	0.08	0.08	4.8	85	150	345	11	20
E	Irrawaddy	Nyaungdoun	80–125 µm	75.5	9.4	4.9	1.3	2.3	1.5	1.5	1.3	0.11	0.08	1.8	51	174	249	12	36
E	Irrawaddy	Nyaungdoun	125–180 µm	77.4	10.3	3.1	1.1	1.3	1.7	2.1	0.4	0.06	0.04	2.4	75	167	342	7	12
E	Irrawaddy	Nyaungdoun	180–250 µm	75.0	11.1	4.0	1.3	0.9	1.5	2.5	0.4	0.07	0.06	3.0	103	161	414	7	12
E	Irrawaddy	Nyaungdoun	Finer bar	76.8	10.1	3.6	1.2	1.5	1.6	2.0	0.6	0.08	0.06	2.4	73	165	332	9	18
E	Irrawaddy	Nyaungdoun	Finer bar	77.1	10.2	3.5	1.2	1.5	1.6	2.0	0.6	0.06	0.05	2.0	74	169	362	8	16
E	Irrawaddy	Nyaungdoun	Coarser bar	81.8	8.1	2.6	0.8	1.1	1.2	2.3	0.4	0.04	0.05	1.5	78	134	395	5	14

La	Yb	Th	U	Zr	Hf	V	Nb	Ta	Cr	Co	Ni	CIA	WIP	CIA/WIP	aAlNa	Eu/Eu*
ppm	ppm	ppm	ppm	ppm	ppm	ppm	ppm	ppm	ppm	ppm	ppm					
67	2.7	36	5	358	10	206	10	0.8	376	13	49	48	51	0.9	1.5	0.54
92	4.0	52	7	248	7	78	18	2.3	27	7	<20	54	55	1.0	1.5	0.37
55	2.5	28	4	145	4	85	11	1.2	89	9	27	53	54	1.0	1.5	0.57
60	3.0	32	5	348	10	101	12	1.3	137	10	32	53	56	0.9	1.4	0.51
33	1.6	15	2	114	3	54	7	0.8	68	6	25	53	50	1.1	1.4	0.61
35	1.5	15	2	90	3	49	6	0.6	55	5	<20	52	49	1.1	1.4	0.61
13	0.6	4	1	63	2	26	4	0.2	75	5	46	57	24	2.4	1.8	0.82
13	1.2	4	1	112	3	74	6	0.3	205	18	116	72	23	3.1	2.1	0.71
9	0.8	3	1	54	2	24	3	0.2	41	5	36	57	26	2.2	1.8	0.86
14	1.0	6	1	93	3	36	4	0.4	75	7	44	57	34	1.7	1.6	0.76
28	2.3	10	2	252	7	88	10	0.8	226	17	91	64	39	1.6	1.8	0.67
37	1.8	15	2	292	7	67	9	0.8	342	11	60	57	36	1.6	1.6	0.57
29	2.2	11	2	333	8	91	9	0.8	260	15	79	61	40	1.6	1.6	0.65
29	1.4	10	1	85	2	51	7	0.6	185	9	52	55	34	1.6	1.6	0.69
11	0.8	4	1	65	2	46	3	0.3	55	8	50	58	37	1.6	1.5	0.80
17	1.1	6	1	88	2	45	5	0.5	89	9	50	56	35	1.6	1.5	0.74
37	3.1	16	3	237	6	127	13	0.9	239	25	135	72	36	2.0	3.4	0.68
29	2.2	11	2	250	6	92	9	0.9	226	17	97	66	39	1.7	1.9	0.69
65	3.6	24	4	693	19	103	19	1.9	910	12	60	54	35	1.6	1.5	0.52
22	1.2	6	1	78	2	51	6	0.5	116	11	63	59	39	1.5	1.5	0.80
17	1.1	5	1	69	2	56	6	0.4	68	16	88	62	41	1.5	1.7	0.86
29	1.8	13	2	272	7	69	9	0.7	383	11	70	58	39	1.5	1.5	0.66
31	2.0	13	2	276	7	65	10	0.9	315	12	65	58	39	1.5	1.5	0.65
30	1.5	10	1	134	4	48	7	0.7	253	8	45	56	35	1.6	1.6	0.64

Table 2. Key geochemical parameters of Irrawaddy sand bars and silty levee sands. The Eu anomaly Eu/Eu* is the measured chondrite-normalized Eu value over the value that Eu would have in a linear extrapolation between chondrite-normalized values of Sm and Gd. Full dataset provided in Appendix Table A4.

	#	Q	F	Lv	Lc	Ls	Lm	TOT	CIA	CIX	WIP	α^{Al}Mg	α^{Al}Ca	α^{Al}Na	α^{Al}K	α^{Al}Rb	α^{Al}Sr	La_N/Yb_N	La_N/Sm_N	Gd_N/Ho_N	Ho_N/Yb_N	Eu/Eu*
Indus	21	**48**	**23**	**2**	**11**	**6**	**10**	100.0	**41**	**70**	**69**	**0.7**	**0.4**	**1.8**	**1.0**	**0.7**	**1.4**	**9.7**	**3.7**	**1.6**	**1.0**	**0.67**
		4	*4*	*1*	*3*	*2*	*3*		*2*	*2*	*5*	*0.1*	*0.0*	*0.2*	*0.0*	*0.1*	*0.2*	*0.3*	*0.1*	*0.0*	*0.0*	*0.03*
Ganga	14	**67**	**15**	**0**	**6**	**4**	**8**	100.0	**46**	**68**	**42**	**0.9**	**0.7**	**1.7**	**0.9**	**0.6**	**2.0**	**10.2**	**3.8**	**1.6**	**1.0**	**0.44**
		3	*3*	*1*	*2*	*1*	*3*		*3*	*3*	*7*	*0.2*	*0.1*	*0.4*	*0.2*	*0.2*	*0.2*	*1.9*	*0.1*	*0.2*	*0.1*	*0.12*
Brahmaputra	17	**61**	**25**	**1**	**0**	**3**	**9**	100.0	**53**	**66**	**46**	**1.1**	**1.2**	**1.3**	**1.0**	**0.7**	**1.3**	**10.7**	**4.0**	**1.5**	**1.0**	**0.60**
		4	*5*	*1*	*0*	*1*	*3*		*3*	*3*	*5*	*0.3*	*0.3*	*0.2*	*0.1*	*0.1*	*0.3*	*1.8*	*0.3*	*0.2*	*0.1*	*0.10*
Irrawaddy	8	**62**	**20**	**3**	**0**	**10**	**6**	100.0	**57**	**66**	**35**	**1.5**	**1.8**	**1.6**	**0.8**	**0.7**	**1.3**	**10.9**	**4.6**	**1.6**	**1.0**	**0.67**
		2	*2*	*1*	*0*	*2*	*1*		*1*	*2*	*2*	*0.3*	*0.4*	*0.1*	*0.1*	*0.1*	*0.0*	*1.7*	*0.5*	*0.1*	*0.1*	*0.08*
Salween	11	**52**	**8**	**0**	**4**	**16**	**20**	100.0	**39**	**68**	**52**	**0.7**	**0.4**	**1.7**	**0.9**	**0.6**	**1.5**	**9.2**	**4.3**	**1.6**	**1.1**	**0.49**
		13	*6*	*0*	*4*	*19*	*10*		*8*	*4*	*6*	*0.5*	*0.5*	*0.5*	*0.1*	*0.2*	*0.5*	*8.8*	*1.8*	*0.3*	*0.1*	*0.14*
Mekong	18	**68**	**5**	**1**	**1**	**11**	**14**	100.0	**70**	**75**	**28**	**1.4**	**3.5**	**2.8**	**1.1**	**0.7**	**2.4**	**9.3**	**3.9**	**1.7**	**1.0**	**0.61**
		11	*6*	*1*	*2*	*7*	*8*		*13*	*4*	*14*	*0.3*	*3.9*	*1.8*	*0.3*	*0.3*	*1.1*	*2.2*	*0.4*	*0.2*	*0.1*	*0.13*
Red River	22	**66**	**5**	**0**	**1**	**13**	**15**	100.0	**59**	**71**	**31**	**1.0**	**1.5**	**2.9**	**0.8**	**0.6**	**2.5**	**9.2**	**4.1**	**1.4**	**1.0**	**0.64**
		8	*5*	*0*	*1*	*6*	*12*		*8*	*5*	*11*	*0.6*	*1.2*	*2.2*	*0.2*	*0.1*	*1.0*	*10.3*	*2.3*	*0.2*	*0.1*	*0.08*
SE China	5	**65**	**19**	**13**	**0**	**1**	**1**	100.0	**60**	**62**	**36**	**5.0**	**6.5**	**2.7**	**0.5**	**0.4**	**2.3**	**8.3**	**4.5**	**1.3**	**0.8**	**0.59**
		16	*5*	*13*	*0*	*1*	*2*		*2*	*2*	*12*	*2.5*	*3.9*	*0.8*	*0.1*	*0.1*	*0.5*	*3.1*	*0.8*	*0.2*	*0.1*	*0.04*
Taiwan	23	**35**	**4**	**2**	**3**	**41**	**16**	100.0	**60**	**73**	**44**	**1.3**	**1.6**	**2.0**	**1.1**	**0.8**	**2.2**	**11.0**	**4.0**	**1.7**	**1.1**	**0.68**
		17	*2*	*1*	*3*	*20*	*11*		*15*	*3*	*14*	*0.5*	*4.2*	*0.9*	*1.4*	*3.0*	*0.9*	*4.0*	*0.6*	*0.3*	*0.0*	*0.12*
Yangtze	42	**53**	**24**	**5**	**4**	**8**	**5**	100.0	**39**	**70**	**58**	**0.6**	**0.4**	**1.7**	**1.1**	**0.8**	**1.4**	**9.4**	**3.8**	**1.8**	**1.1**	**0.70**
		7	*2*	*1*	*5*	*4*	*2*		*11*	*5*	*12*	*0.4*	*0.8*	*1.3*	*0.2*	*0.3*	*0.8*	*3.4*	*0.8*	*0.2*	*0.1*	*0.11*
Yellow River	5	**52**	**31**	**2**	**8**	**4**	**3**	100.0	**38**	**63**	**56**	**1.1**	**0.5**	**1.1**	**0.9**	**0.8**	**1.0**	**8.0**	**3.7**	**1.6**	**1.0**	**0.65**
		2	*4*	*1*	*3*	*2*	*1*		*6*	*2*	*5*	*0.2*	*0.2*	*0.2*	*0.2*	*0.1*	*0.2*	*0.6*	*0.1*	*0.0*	*0.1*	*0.07*

Table 3. Main petrographic and geochemical parameters of river sands from southern and eastern Asia (mean in bold, standard deviation in italics). Lc = carbonate lithics; other petrographic pa- rameters as in Fig. 4. CIA, WIP and αAl values are not corrected for Ca and Mg in carbonates to emphasize the distinction between river sands containing few or no carbonate grains (Ir- rawaddy, Brahmaputra, Mekong, Red River, SE China rivers) and Indus, Salween, Yangtze and Yellow River sands containing significant limestone and dolostone rock fragments and thus characterized by CIA ~40, αAlMg as low as 0.6–0.7 and αAlCa b 0.5. Intermediate indices characterize Ganga sand also containing carbonate grains. Comparison of various parameters in- dicate strongest weathering for Mekong, Red River and SE China catchments. Sources as for Fig. 8, also including data after Garzanti et al. (2005), Nie et al. (2015) and Garzanti and Resentini (2016).